University of Massachusetts Amherst
ScholarWorks@UMass Amherst

Masters Theses | Dissertations and Theses

October 2019

Optical-Fiber-Based Laser-Induced Cavitation for Dynamic Mechanical Characterization of Soft Materials

qian feng

Follow this and additional works at: https://scholarworks.umass.edu/masters_theses_2

 Part of the Materials Science and Engineering Commons, and the Mechanical Engineering Commons

Recommended Citation

feng, qian, "Optical-Fiber-Based Laser-Induced Cavitation for Dynamic Mechanical Characterization of Soft Materials" (2019). *Masters Theses*. 830.
https://scholarworks.umass.edu/masters_theses_2/830

This Open Access Thesis is brought to you for free and open access by the Dissertations and Theses at ScholarWorks@UMass Amherst. It has been accepted for inclusion in Masters Theses by an authorized administrator of ScholarWorks@UMass Amherst. For more information, please contact scholarworks@library.umass.edu.

OPTICAL-FIBER-BASED LASER-INDUCED CAVITATION FOR DYNAMIC MECHANICAL CHARACTERIZATION OF SOFT MATERIALS

A Thesis Presented

by

QIAN FENG

Submitted to the Graduate School of the
University of Massachusetts Amherst in partial fulfillment
of the requirements for the degree of

MASTER OF SCIENCE
IN
MECHANICAL ENGINEERING

September 2019

Mechanical and Industrial Engineering

OPTICAL-FIBER-BASED LASER-INDUCED CAVITATION FOR DYNAMIC MECHANICAL CHARACTERIZATION OF SOFT MATERIALS

A Thesis Presented

by

QIAN FENG

Approved as to style and content by:

_____
Professor Jae-Hwang Lee, Chair

_____
Professor Tingyi Liu, Member

_____
Professor Jinglei Ping, Member

_____
Sundar Krishnamurty, Department Head
Mechanical and Industrial Engineering

ACKNOWLEDGMENTS

I would like to thank my advisor, Prof. Jae-Hwang Lee, for his two years of patient guidance and instruction. I would also like to extend my gratitude to the members of my committee, Prof. Tingyi Liu and Prof. Jinglei Ping, for their comments of my project.

A special thanks to Sacchita Tiwari, Wanting Xie, and Swetaparna Mohanty for their support and contribution in the project.

This research was partially supported by the Office of Naval Research under grant N00014-17-1-2056 (Dr. Timothy Bentley).

ABSTRACT

OPTICAL-FIBER-BASED LASER-INDUCED CAVITATION FOR DYNAMIC MECHANICAL CHARACTERIZATION OF SOFT MATERIALS

SEPTEMBER 2019

QIAN FENG, B.A., HARBIN ENGINEERING UNIVERSITY

M.S., UNIVERSITY OF MASSACHUSETTS AMHERST

Directed by: Professor Jae-Hwang Lee

In the laser-induced cavitation (LIC) technique, a vapor-gas cavity is generated in water, or a soft material by focusing an intense laser pulse into the sample. The high-strain-rate mechanical properties of these samples can be investigated through a real-time size measurement of the expanding cavity bubble. Although this LIC technique has been applied to multiple research fields such as mechanical, biological and medical areas. It is possible to simplify and improve this LIC method by introducing optical-fibers. In this approach, we propose to employ an optical-fiber to deliver the intense laser pulse to an arbitrary position of an optical opaque specimen. At the same time, we also attempt to generate LIC at one end of the optical-fiber. This optical-fiber based LIC is achieved by dip-coating of the laser absorbing film on the fiber end. Thus, the film can absorb the laser pulse and generate LIC within the sample.

In this study, the development of the coating material, the introduction of the optical-fiber into the existing LIC system, and the optical-fiber based LIC experiments are performed to characterize high-strain-rate mechanical properties of soft materials. We investigate the coating conditions and verify the consistency of the ablation based on the

optimized coating materials. By conducting LIC experiments with gelatin samples, the feasibility of developed LIC method is investigated, LIC events are successfully formed at the fiber end which is inserted into the sample, and the rapid expanding dynamics are imaged with ultrafast stroboscopic microscopy. Using the multiple-exposure images, the expanding speeds and maximum cavity sizes are quantified to provide high-strain-rate characteristics of the soft materials. The inconsistency of the cavitation behavior resulted by the fluctuation of the coating condition and the high power intense laser conducting optical-fiber destruction can be improved by developing new coating method and new protective coating on the fiber end in the future.

TABLE OF CONTENTS

Page

LIST OF TABLES

LIST OF FIGURES

CHAPTER 1

INTRODUCTION

1.1 Research background and significance

Mechanical properties are physical properties used to describe the behaviors of material under various mechanical properties, including hardness (Xiaodong Li, 2003), tensile strength (Anna Bellini and Selçuk Güçeri, 2003), yield strength (Erik T Thostenson and Tsu-Wei Chou, 2002), Young's modulus (Staffan Greek, 1999), etc. Soft materials are materials that can be easily deformed by thermal or mechanic stress. Strain-rate is the strain changing which is respect to time. The same materials at high and low strain-rate may perform differently. To understand and apply materials appropriately, it is important to study their mechanical properties using the mechanical characterization approach. For examples, non-destructive pull force test (Bartosz Kawa, Jun 2018), tension-compression test (Richard K. Boger, 2005), nanoindentation approach (Zhiwen Chen, Dec 2018), etc. However, most methods are adequate for ascertaining the hardness of materials. As for soft materials, especially, for those that behave differently at a high-strain-rate such as tissues and hydrogels, there are characterization limits due to their wnique properties. When soft materials experience a high stain-rate, slow shear wave speed, high compliance, and non-linear viscoelasticity, these are the main phenomena that lead to difficulty analyzing these types of materials (Jonathan B. Estrada, 2018). The introduction of laser-induced cavitation (LIC) can overcome most of these limitations in the study of high-strain-rate soft materials. However, there are limitations in the current LIC system. In the current LIC, the cavitation is generated by focusing an intense laser pulse on the sample's surface or in the middle of

a transparent sample (Sung-Yong Park, 2011), which means the cavitation cannot be induced without a high-focus intense laser pulse or in the middle of an opaque sample. Thus, an advanced LIC is being developed which use an optical-fiber to overcome these disadvantages.

1.1.1 Current mechanical characterization approaches

As it is paramount to study mechanical properties of materials, many approaches have been developed to describe the mechanical properties of materials. However, there are limitations to every approach for different kinds of material or different properties. Not all the approaches are a good-fit for every material. The classic approaches, including tension-compression experiment work well when estimating macroscopic length scale materials, for example, sheet material (Richard K. Boger, 2005). However, this approach is more focused on providing information on materials at macroscopic length scales. Meanwhile, the classic Johnson–Kendall–Roberts (JKR) theory with small-scale techniques allows for small scale samples but fails at non-linear viscoelasticity's samples (Robert W. Style, 2013). Alternatively, the development of pressure-induced cavitation reveals more detailed properties inside the soft materials (Jessica A. Zimberlin, 2007a). However, this approach can only analyze soft materials at low or medium strain-rate (10^{-4} – 10^{2} s^{-1}). It is limited when this approach is extended to a faster loading speed in order to characterize high-strain-rate (10^{3} – 10^{8} s^{-1}) soft materials because of hardware and insufficient frameworks (R. W. Klopp, 1985). However, using inertial cavitation allows for investigation of these kinds of soft materials, since, in essence, inertial cavitation is a type of cavitation where microbubbles rapidly expand and violently collapse (Christorpher Earls Brennen, 2014). Meanwhile, laser-induced cavitation, inertial cavitation generated by laser,

is an alternative experimental technique that can be used to examine local mechanical properties of soft materials by measuring the radii of cavitation bubbles (Jessica A Zimberlin, 2010) when regulated laser energy is applied, and subsequently at the transition from cavitation to fracture (Jessica A. Zimberlin, 2007b; Santanu Kundu and Alfred J. Crosby, 2009). Accurately, the mechanical properties can be determined by the amplitude, frequency, and decay of cavitation oscillatory behavior. **Figure 1.1** shows the evolution of the approaches used to characterize soft materials, for microscopic, and macroscopic scales, respectively at low and high-strain-rate. LIC is the most-fit approach used to analyze soft material undergoing high-strain-rate at a microscopic scale.

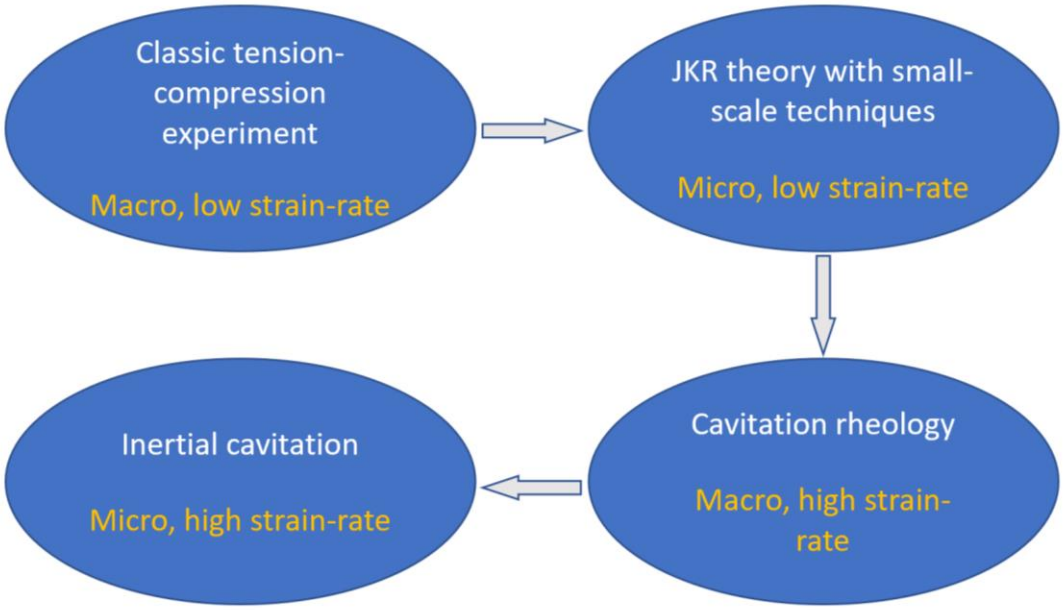

Figure 1.1 Evolution of soft material's characterization

1.1.2 Current applications of laser-induced cavitation

Laser-induced cavitation (LIC) is a process where a laser is employed to generate a cavitation bubble in a sample after absorbing optical energy from the laser pulse. The LIC can be developed to conduct various experiments as well as be applied in several research fields including mechanical, medical and biological studies (Apostolos G. Doukas,

1993; Roeland Jozef Gentil De Moor, 2009; Tetsuya Kodama and Kazuyoshi Takayama, 1998). Measuring soft material's strain, stress and other dynamics properties (Emil-Alexandru Brujan, 2001) is just one of the applications of the LIC. Particularly, the LIC can be used to clean the surface by removing particles from the surface as the bubble is expanding. By focusing an intense laser pulse into the water placed in a cuvette with a microscope slide located on the bottom of the cuvette serving as the target surface. The cavity bubble generated will expand and collapse on the target surface. The cavitation process removes the grease-particle mixture on the surface from the center (**Figure 1.2**) (Claus-Dieter Ohl, 2006). In medical and biological applications, several discoveries are based on various kinds of cavitation. The cerebrospinal fluid (CSF) cavitation caused by blasts with high impulses plays an important role in brain tissue injury (Matthew B. Panzer, 2012). Ultrasound-induced intramembrane cavitation could underlie the biomechanics of acoustic therapeutic treatments (Michael Plaksin, 2014), temporary cavitation created by gunshot wounds probably produces axonal and neuronal damage extending around 18mm (Manfred Oehmichen, 2000). However, these brain-related cavitation studies can be stimulated and analyzed in the LIC system. This also makes the LIC a very important and

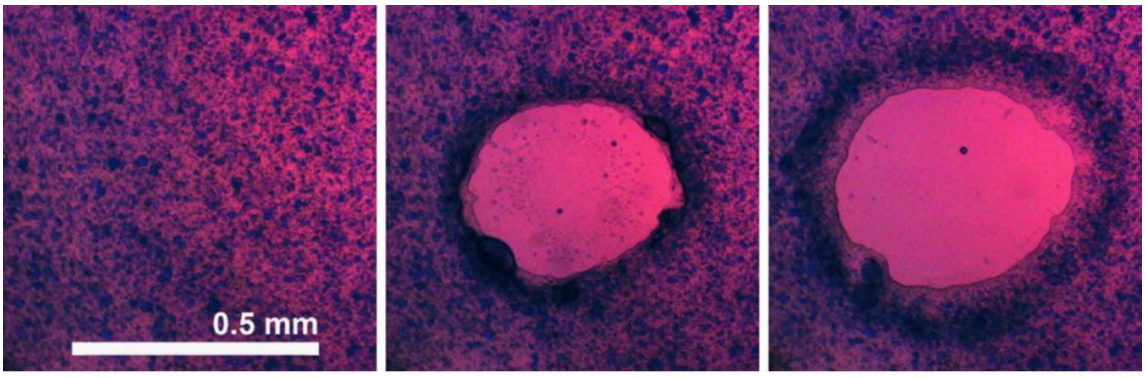

Figure 1.2 The grease-particle mixture is removed from the center by the cavitation (Ohl, 2006)

necessary experimental method that can be used to investigate the mechanical behavior of various high stain-rate soft materials including brain tissue.

1.2 Introduction of laser-induced cavitation

The LIC system is important for researchers to study the mechanical behaviors of high-strain-rate soft materials. **Figure 1.3** shows the fundamental components of the LIC system. The cavitation is generated by absorbing energy from the Nd:YAG laser. With the illumination of the stroboscopic illumination laser pulse, the camera can record the expanding process of the cavitation as a multiple exposure image.

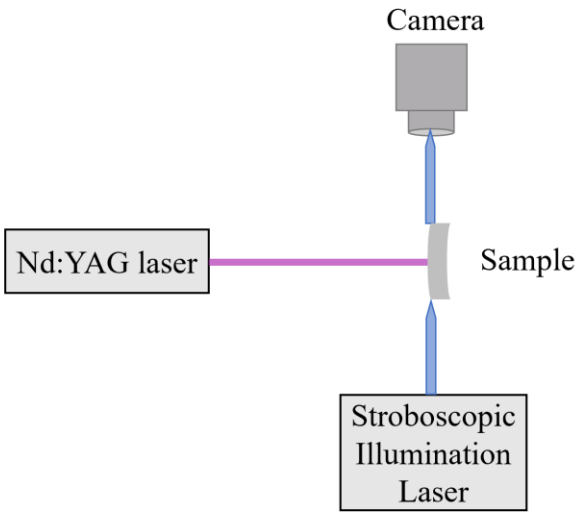

Figure 1.3 Fundamental Components of the LIC system

1.2.1 Nd:YAG laser

In the laser-induced cavitation system, the cavity is generated by highly-focusing an intense laser pulse into the sample. The laser used for cavitation generation here is the Nd:YAG laser which is the abbreviated form of the neodymium-doped yttrium aluminum garnet laser which is a solid-state laser. The Nd:YAG is a crystal where the neodymium dopant is around 1% of yttrium ions in the YAG crystal that is used as an active medium in the laser system. The YAG ($Y_3Al_5O_{12}$) crystal is stable and optically isotropic, which

makes it have low optical loss and high optical perfection than other laser mediums. The property, which has good compatibility, is comprised of substituted trivalent ions of rare-earth and iron groups and provides YAG the ability to accept the trivalent neodymium dopant (J. E. Geusic, 1964). The electrons of the trivalent neodymium ions at lower energy state are excited to the higher energy state to achieve population inversion and provide lasing action (Alexander S. Zibrov, 1995).

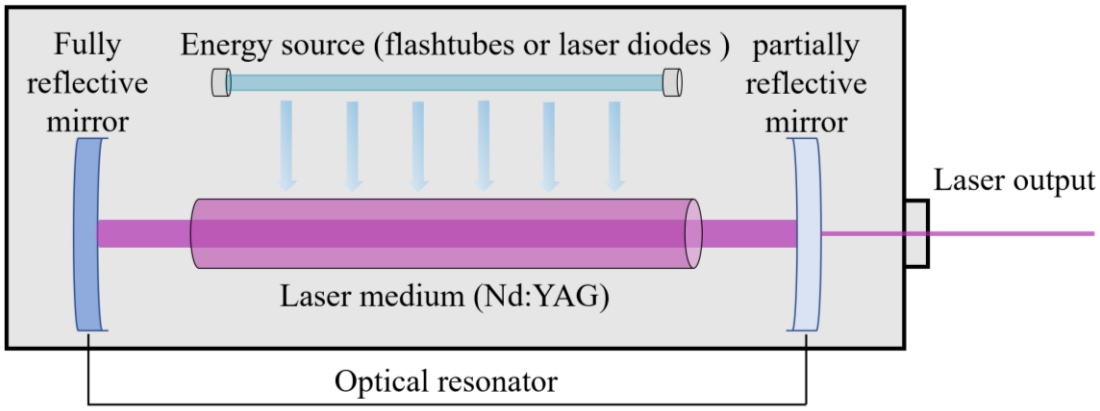

Figure 1.4 Construction of the Nd:YAG laser

In the Nd:YAG laser construction (**Figure 1.4**), the laser system consists of 3 elements where Nd:YAG crystal is the active medium. The other two components are the energy source and optical resonator which can cooperate with the active medium to achieve the laser generating function. The most common laser sources are flashtubes or laser diodes (Monte Ross., 1968). The energy from the source is pumped into the grain medium, which is a YAG crystal, with a lower absorption. The neodymium dopant which has higher absorption absorbs the energy from the source and achieve transitions to provide lasting action. The host crystal is placed between the optical resonator which includes two mirrors, and these two mirrors are silvered or coated completely and partially, respectively. The light is fully reflected by the fully reflective mirror, meanwhile, the partially reflective

mirror reflects most of the light. Hence a small portion of light can pass through the partially coated mirror and forms the laser beam (Herwig Kogelnik and Tingye Li, 1966).

1.2.2 Cavitation recording

To characterize the mechanical behavior of materials based on LIC, recording the cavitation process is the first step. However, the interval of expanding, collapsing and oscillating processes are around a hundred microseconds, which make the recording very challenging with standard recording strategy. There are, commonly, two approaches to record the short interval event, which employ an ultrahigh-speed camera or with the cooperation of the stroboscopic laser pulse. On one hand, with minimal shutter time and exposure time, the high-speed camera can achieve a frame rate of up to 200 million frames per second (fps) (Emil-Alexandru Brujan and Yoichiro Matsumoto, 2012). The most current ultrahigh-speed camera can even achieve the frame rate of 10 trillion fps (Jinyang Liang and Lihong V. Wang, 2018). However, to make an ultrahigh capture speed, properties including sensitivity, dynamic range, and linearity may be traded off (Edoardo Charbon, 2004). On the other hand, the camera can capture the cavitation behavior with the illumination of the stroboscopic laser pulse. The stroboscopic laser pulse can provide a continuously high-repetition-rate, a short-pulse laser which can be used to illuminate the sample in the cavitation process (Rie Tanabe, 2015). The camera can start the image acquisition while the laser pulses are delivered into the camera (Wanting Xie, 2017). Due to the consistent and continuous laser pulse, the cavitation process can be recorded consistently as multiple-exposure images. Meanwhile, the cavitation magnitude, varying duration and expanding speed information can be recorded by the multiple-exposure image.

Consideration for the practicality and cost, the high-speed strobe laser is employed to illuminate the sample for the recording in our studies.

1.2.3 Cavitation process

1.2.3.1 Cavity generation

In the LIC, the cavitation is generated by a laser, for which this system is called laser-induced cavitation. However, in the general mechanical characterization based on single cavitation, there are two means of cavity generation methods which are spark generation based on electrical discharging and optical generation based on the laser (Iskander Sh Akhatov, 2001). In the spark generation method, the cavity bubble is produced in water by passing a large short duration current through a short wire which is nicked to form a constriction. A powerful potential is generated when the current passes through the constriction and part of the wire, which results in a spark and vaporizes the water to form a cavity bubble (Mark Harrison, 1952). On the other hand , in the optical generation, an intense laser pulse is focused on the target sample, the focal region becomes extremely hot after absorbing the laser energy. Then, local breakdowns occur on the sample and a plasma is produced at the target region (B. Ward and D.C. Emmony, 1990; M. P. Felix and A. T. Ellis, 1971). Subsequently, more laser energy can be absorbed to vaporize water and form cavitation. However, the bubble dynamics can be influenced mainly by the electrodes in the spark generation method; the laser generation has become the primary method that is extensively used in mechanical characterization of materials (Iskander Sh Akhatov, 2001).

1.2.3.2 Cavity expansion process

After the cavitation is generated in the sample by the highly-focused intense laser pulse, the cavity bubble rapidly expands and achieves the maximum radius. At this point, the gas pressure in the bubble is much less than the pressure of the liquid outside of the bubble, which leads the bubble to contract. In the contraction process, the gas inside the bubble heats up, and in turn heats the bubble wall. This is accompanied by the condensation of the vapor inside the bubble. At the critical point, the temperature reaches its peak and stops rising, and this process is accompanied by the compression of the noncondensable vapor, which causes a rapid increase of the vapor pressure. Hence, the bubble rebounds as it stops contracting (Iskander Sh Akhatov, 2001). This process repeats several times until it reaches equilibrium. Thus, in the cavitation process, the cavity bubble expands, collapses, and subsequently oscillates after the cavity is generated (**Figure 1.5**). The mechanical properties can be characterized based on this process.

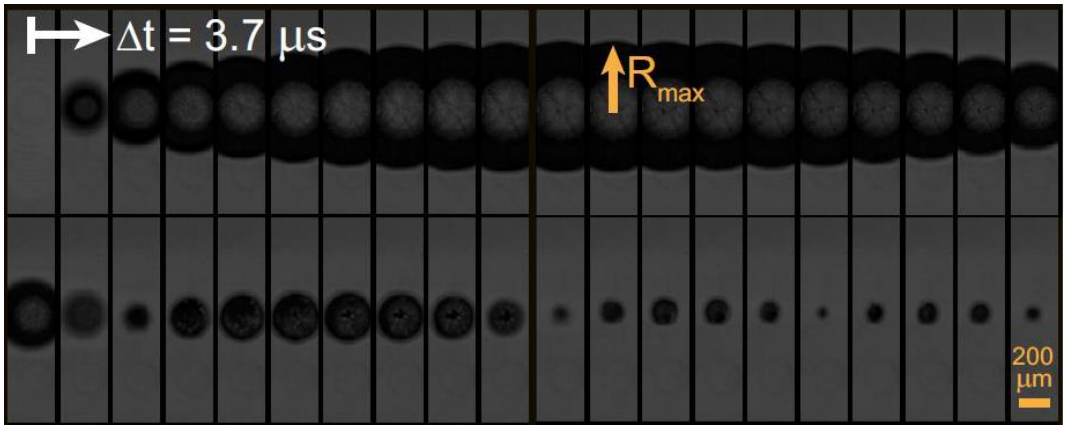

Figure 1.5 Cavitation varying process (Estrada, 2018)

1.3 Introduction of optical-fiber

With the LIC system, soft materials at high-strain-rate can be characterized mechanically. However, this approach is limited when describing transparent objects. Inn an opaque sample, cavitation can be produced more efficiently. An optical-fiber is

introduced into the system and cooperates with the ablation laser to generate cavitation on the fiber's end surface. The optical-fiber is flexible and transparent and is able to deliver light from one end to the other. It can be used as a medium to transmit the information as a light pulse with less loss and higher bandwidth than metal wires (John M. Senior and M. Yousif Jamro, 2009).

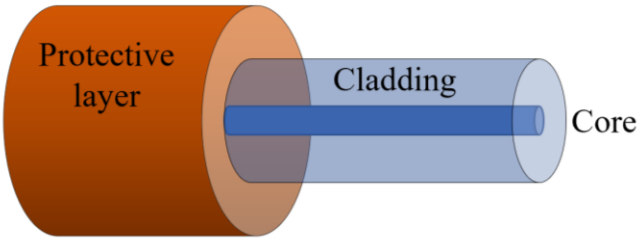

Figure 1.6 Construction of optical-fiber

Generally, optical-fibers made by glass or plastic will consist of the fiber core, cladding, and some protective layers. **Figure 1.6** shows the construction of typical optical-fiber. The fiber core is in the center and surrounded by the cladding layer. The protective layer is coated outside the cladding. The reflective index of the fiber core is higher than the cladding's, which can keep the light propagating in the core by the total internal reflection phenomenon. Optical-fibers can be classified as multi-mode fibers and single-mode fibers depending on the number of propagation paths. Typically, multi-mode fibers have a wider core radius and shorter propagation distance to support more propagation path. Whereas, single-mode fibers are used to deliver one single path, which makes it have a smaller radius and can support a long propagation distance. Additionally, a laser is commonly used as the light source for single-mode optical-fibers.

1.4 Previous work

The LIC system has been widely applied in the mechanical characterization of high-strain-rate soft materials. The laser is used to generate a cavitation bubble, which can

be recorded by a camera, and the mechanical properties can be analyzed based on the recorded cavitation behavior. In the previous studies, a high-focused intense laser is used to achieve dielectric breakdown and form a plasma which will, in turn, absorb the laser energy and generate a cavity in the soft material or liquid samples (Iskander Sh Akhatov, 2001). The expanding image of the cavitation bubble can be recorded by ultrafast stroboscopic imaging (Qiyong Chen, 2018) or a high-speed camera. However, the laser pulse is required to be high-focused and intense to achieve the dielectric breakdown and form the plasma phase, which makes the experiment condition more complicated (A. G. Molchanov, 1970). Additionally, the cavitation process based on the dielectric breakdown of the sample medium can be initially unstable because of the nonlinearity of the dielectric breakdown. Furthermore, the gas inside the cavitation formed by the evaporated medium is various in different samples, which can affect cavitation behavior as well.

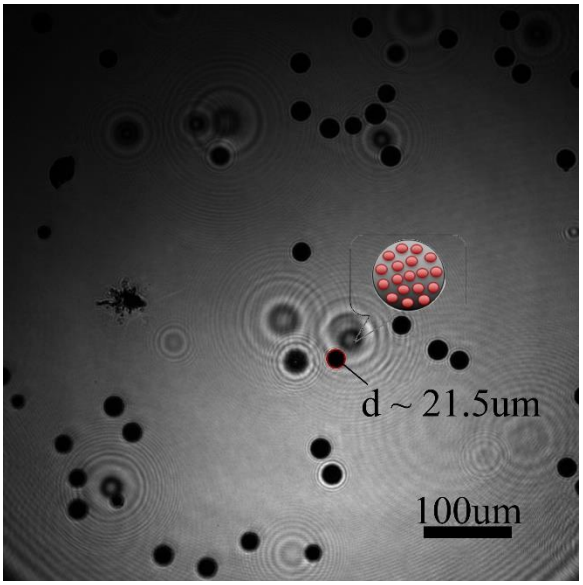

Figure 1.7 Microscopic image of the laser-absorbing seeds
and the construction diagram

In order to achieve the cavitation with lower laser power and exclude the influence by the unstable dielectric breakdown, our group has developed a seeded LIC system, in which seed particles are placed in the sample to reduce the required laser power by making

the seed particles absorb laser energy rather than using the high-focused intense laser to achieve dielectric breakdown and form plasma phase to absorb laser energy. The seed particles consist of polymeric particles that can vaporize to form cavitation, which can ensure the cavity bubble is formed by the same material in different samples. The seed particle is around 22um diameter and structured by a polystyrene molecule in the center and surrounded by several dye particles (**Figure 1.7**). The dye particles can absorb energy from the laser and heat the polystyrene molecule up to vaporize. However, the seed particles are not easy to be placed in the interior of the established sample if the seeds are not blended with the sample at initial-preparation. Besides, even if the seed particles are placed in the interior of the sample, the laser energy may change when the focal point is in different positions if the sample is not entirely transparent.

1.5 Research goal and main tasks

The aim of this study is to develop and improve the LIC system that could be utilized in more applications, and an optical-fiber is introduced in the advanced LIC system. The optical-fiber is used to propagate the ablation laser and deliver it to the cavitation position in the sample. The coating materials are coated on the fiber end to conduct cavitation based on this end. The feasibility of this system will be investigated, and the mechanical behavior of gelatin will be investigated preliminarily.

First, the coating materials were identified to find the optimal mixture of the laser-absorbing dye and polymeric material. Also, the coating condition was investigated by determining the relationship between the coating thickness and solution concentration. Moreover, the feasibility of the solution was investigated by the ablation experiment.

Second, the advanced LIC system was set up. The coating materials in different conditions were investigated by the cavitation experiment with different samples. The optimal composition of the laser-absorbing material was identified. Subsequently, the consistency of the advanced LIC system was verified. The mechanical behavior of different samples was contrasted as well.

The improvement of the LIC system can expand the application of the LIC into the interval of the sample. Moreover, this development can improve the consistency of the LIC experiment.

CHAPTER 2

OPTIMIZATION OF COATING MATERIALS AND COATING CONDITIONS

2.1 Abstract

To conduct cavitation on the end of optical-fiber with reduced laser energy, coating materials including laser absorbing dye and evaporating polymer used to vaporize should be coated on the end surface. The coating materials were investigated by the microscopic observation on the spin-coated alternative solutions to find the optimal ingredients including dye, polymer, and solvent. The optimal solution should be transparent and uniform. Hence, IR165 was selected as a laser dye from substitutes, including carbon nanopowder and resin colorant. Polystyrene was determined as the polymer in the laser absorbing coating material. In the solvent alternatives, which include acetone, chloroform, ethanol, dimethylformamide (DMF), toluene, and isopropyl alcohol (IPA), cyclopentanone was verified as the optimal one. The selected solution was investigated by the laser-induced ablation and the feasibility and consistency of conducting LIC were verified. Subsequently, the coating condition was investigated with a 3D optical profilometer to define the solution's concentration and coating thickness curve at a certain spin speed. The thickness monotonically increases when increasing the solution's concentration at certain spin speed. At the same level, the coating thickness is larger when the spin speed is increased. Therefore, the coating thickness from the dip-coating should be greater than those by spin coating. Meanwhile, the coating thickness should be increased when the increasing the solution's concentration.

2.2 Introduction

From the LIC based soft material's mechanical properties of previous studies, the object is heated by a high-focused intense laser to achieve dielectric breakdown and to form a plasma. Subsequently, the plasma phase in the sample can absorb even more energy from the ablation laser and create the cavitation by partially vaporizing the sample (A. G. Molchanov, 1970). Nonetheless, the requirement of laser energy is demanding, which is challenging to achieve. In addition, the dielectric breakdown can be nonlinear, which makes the initial stage of the cavitation fluctuate. Moreover, the evaporated medium that forms the cavitation can make the cavitation perform differently amongst various samples. Therefore, to reduce the required laser energy and to improve the consistency, the laser absorbing dye and vaporizing polymer are employed, respectively, in the advanced optical-fiber based laser-induced cavitation system. The laser dye and evaporating polymer are dissolved in a common solvent which can evaporate with an appropriate evaporation rate. With this coating solution, the laser with a certain wavelength can be absorbed by particular laser dye rather than converting the sample to plasma to be absorbed. The initial instability can be avoided without the dielectric breakdown of the sample. Furthermore, the subsequent cavitation performance is able to achieve consistency in a different sample by employing the consistent cavity-forming medium instead of based on the investigated sample. Hence, in the coating materials, laser dye is aimed to absorb energy from the ablation laser. Moreover, the energy can be used to evaporate the polymer on the coating. To conduct cavitation based on the coated optical-fiber, the coating layer on the fiber end has to be transparent and uniform. Thus, cavitation behavior will not be affected by uneven laser absorption. The coating materials will be spin coated on a cover slip to be observed

under 5 times' or 50 times' microscopy to verify the composition of the coating materials. The alternative solution with transparent and uniform microscopic image will be selected as the coating materials which will be subsequently verified with laser-induced ablation. The feasible solution should be able to create consistent ablation trace with specific ablation laser energy.

To study the influence of the coating when altered by adjusting the ratio of the components in the coating materials, the relationship between thickness and PS concentration at various spin speeds was investigated. The coating thickness was measured by a 3D optical profilometer.

2.3 Materials and Method

2.3.1 Preparation of alternative coating solution

The coating solution including laser dye, evaporating polymer and solvent should be able to create a transparent and uniform coating on the fiber end. Analogously, the selected coating solution should be able to create a transparent and uniform coating layer on a glass cover slip (Fisherbrand^{TM}, 25mm x 25mm) by spin coating. Polystyrene (PS, Sigma-Aldrich) was chosen as the evaporating polymer. The carbon, mesoporous (Sigma-Aldrich), black resin colorant (ComposiMold.com) which is a commercial black pigment, and IR165 (Luxottica Exciton) which is an inferred absorber were selected as a laser dye. Acetone (Fisher Scientific), chloroform (Fisher Chemical), ethyl alcohol (ethanol, Pharmco-Aaper), dimethylformamide (DMF, Fisher Chemical), toluene (Fisher Chemical), isopropyl alcohol (IPA, Fisher Chemical), and last cyclopentanone (Alfa Aesar) were considered as available solvents. The alternative solutions were made by measuring a certain amount of laser dye and 0.075 g polystyrene with analytical balance (Mettler

Toledo). Then 1mL solvent measured by 10-100 microliter pipette (Sci Logex) was dropped into the mixture. The solution was blended by a sonicator (Branson 1510) for 20mins, after which the dye and polymer were completely dissolved in the solvent.

2.3.2 Microscopic investigation of alternative solutions

The spin coater (Laurell WS-650MZ-23NPPB) was set up as two steps at 1000 revolutions per minute (RPM) for 20s and a higher expected spin speed for 60s. The first step was aimed to accelerate the spin coater to the expected spin speed ultimately, and the second step was the main spin coating process. A cover slip that was thoroughly rinsed by soap water and water then dried by high-pressure gas was placed on the spin center of the spin coater. By vacuuming the air from the bottom, the cover slip was fixed on the spin center. Then, an alternative coating solution was dropped on the cover slip by pipette. After spinning for 80s, the coated cover slip was observed under FS70 reflection microscopy (Mitutoyo, Japan) at 5 or 50 times' zoom-in to investigate the property of the coating materials. The available coating materials were selected based on the microscopic images. Since the cavitation behavior may change if the laser focal point varies from the assembly part of the black particles to the transparent part. The coating materials that can generate consistent cavitation should be able to create completely transparent and uniform coating on the cover slip.

However, the type and amount of laser dye, the type of solvent, the number of drops on the cover slip, and spin speed may all affect the coating result of alternative solutions. Carbon toner, resin colorant, and IR165 were investigated as the laser absorbing dyes. For each type of dyes, the coating solution with different amount of laser dyes was investigated with 75mg PS and 1ml different organic solvents. 2.5mg, 5mg and 7.5mg dyes were

applied to study the effect of dye content. Two and three drops of coating solutions were applied onto the cover slip by pipette to investigate the impact of applied solution content. 2000RPM and 3000RPM of spin speed were applied to investigate the effect of the spin speed. Different lengths of sonicating time were used to exclude the effect of the dissolving speed.

2.3.3 Verification of laser induced cavitation

The solution of 0.2g PS, 7.5mg IR165, and 1ml cyclopentanone was spin coated on the cover slip by spin coater at 1000RPM for 20s, and 2000RPM for 60s to verify the cavitation feasibility of the coating materials. The coated cover slip was placed on the sample stage of the advanced laser-induced projectile impact test (α-LIPIT, **Figure 2.1**) (Jae-hwang Lee, 2012; Jae-Hwang Lee, 2014) to conduct ablations on the coating layer by specific laser energy. The ablation laser pulse (~5-8ns pulse duration, 1064nm) is produced by a Nd:YAG pulsed laser (Quanta-Ray INDI-40-10-HG, Spectra-Physics) by an external trigger (Wanting Xie, 2017). The ablated coating layer was recorded by the targeting camera as a microscopic image. Ablation traces should appear in the microscopic image with similar sizes to verify the feasibility and the consistency of the coating materials in the LIC.

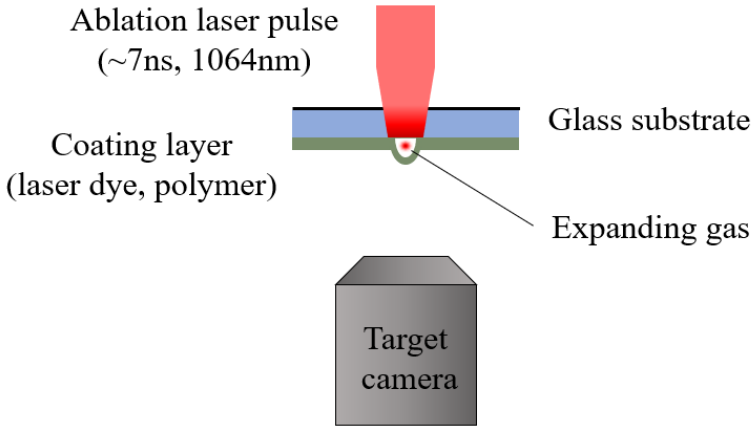

Figure 2.1 The ablation test in the α-LIPIT

2.3.4 Measurement and investigation of coating thickness

The coating solution was prepared in different PS concentrations. 0.2g, 0.4g, 0.6g, 1.0g, 2.0g PS were weighted by analytical balance for solutions of 9%, 16.4%, 23%, 33%, and 50% PS concentrations, respectively. 0.015g laser dye measured by analytical balance and 2ml solvent was dropped by 10-100ul pipette and prepared for the coating solutions. These solutions at different PS concentrations are spin coated on cover slips by the spin coater. The spin speed was at, accelerating speed, 1000RPM first for 20s, and then at, main spin speed, 2000RPM, 4000RPM, and 6000RPM, respectively, for 60s. An approximately 2.5mm scratch was etched by a pair of tweezers on the coated glass substrate down to the surface of the substrate. A 3D optical profilometer (Nexview™ NX2, Zygo) is employed to measure the height difference from the glass substrate to the top coating surface. The PS concentration and coating thickness curve at certain spin speed, and the spin speed and coating thickness curve at PS concentration are plotted by MATLAB to analyze the coating condition of the coating solution and speculate the coating condition of the dip-coating of the fiber.

The 3D optical profilometer (**Figure 2.2**) is an interference microscope (Massig Jurgen, 1989) using a wavelength of light as the ruler. It measures height variations of the surface based on a white light interferometer system (U. Schnell, 1996). In the measuring process, the light beam is split by beam splitter (James C. Wyant, 1984). Half of the beam is reflected to the reference mirror. Whereas, the other half of the beam is delivered to the test surface that is passed through the microscope objective's focal plane. The interference fringes occur in the digital camera image when the distance between the beam splitter and the reference mirror is the same as the distance between the beam splitter and the test

surface. As the reference mirror is practically close to perfect flatness, the difference of the optical path is entirely due to the height difference in the test flat. Therefore, the height variance of the test surface can be calculated by the profilometer based on the interferogram and the wavelength of the light (E. V. Sysoev, 2010).

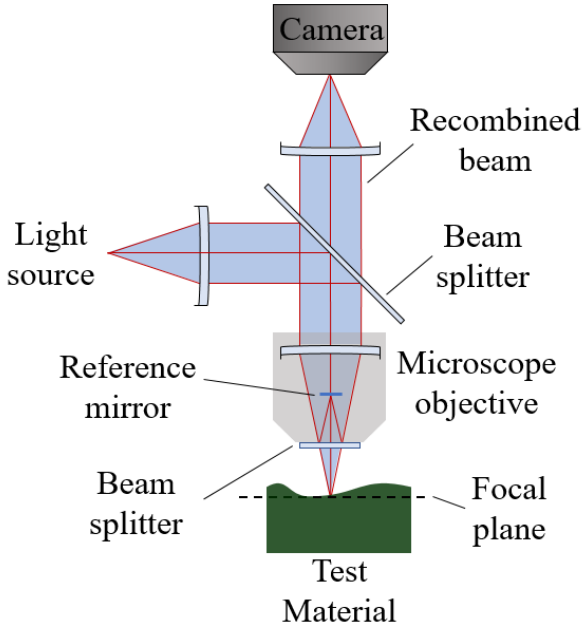

Figure 2.2 Construction of 3D optical profilometer

2.4 Result and Discussion

2.4.1 Investigation of the coating composition

2.4.1.1 Spin coating condition based on carbon toner

The toner was first investigated as a laser absorbing dye. The solutions with acetone, chloroform, IPA, DMF, toluene and ethanol as organic solvents were microscopically observed at 5 times' zoom-in. The carbon nanopowder cannot completely dissolve in all selected organic solvents. There are uneven dark shadow and black spots distributed in the microscopic images. As an example, **Figure 2.3** shows a 5 times' microscope image of spin coated ethanol solution with 2.5mg toner and 75mg PS. Two drops of the solution and 2000RPM of spin speed were applied.

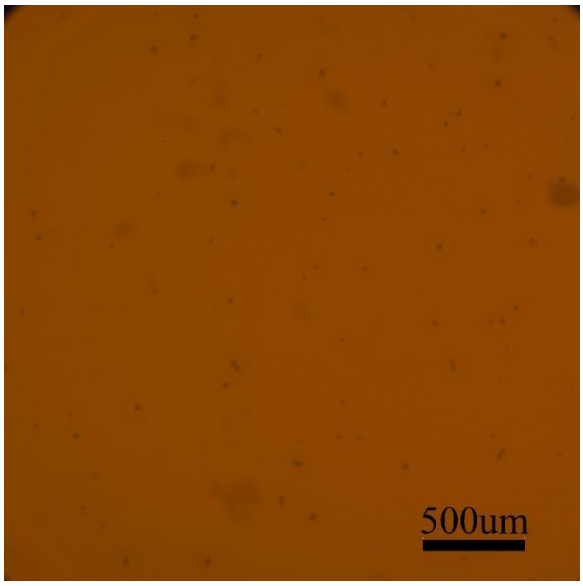

Figure 2.3 5x ethanol solution with 2.5mg toner

Though the toner applied solutions cannot be utilized as the coating solution, coating properties can still be investigated based on these solutions. Two and three drops of the solution were used when investigating the effect of the number of drops. In **Figure 2.4**, the chloroform solution with 1mg toner and 75mg PS was dropped twice and three times on the cover slip, respectively. Then, the cover slip was spin coated at 2000RPM. The magnitude and amount of the black particles were almost the same for different

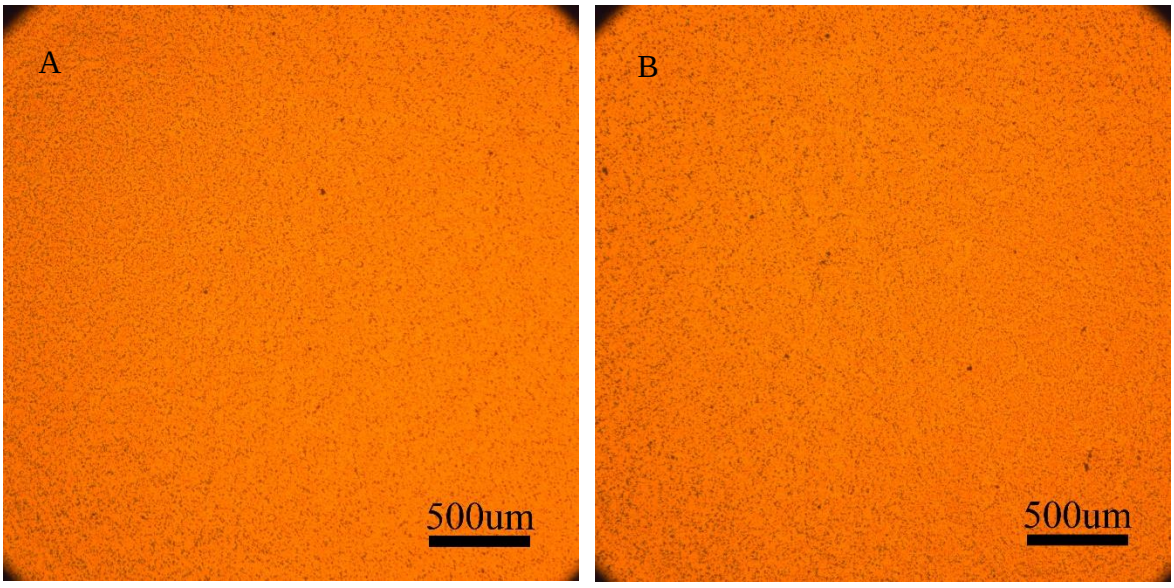

Figure 2.4 5x different drop numbers of chloroform solution with 2.5mg toner (A: Two drops of solution & B: Three drops of solution)

numbers of drops. Hence, the coating condition would not be affected much by different dropping numbers before the spin coating.

The chloroform solution with 2.5mg toner and 75mg PS was dropped twice on the cover slip. The main spin speed was set as 2000RPM and 3000RPM for 60s to investigate the effect of spin speed. The black particles are denser in the 5 times' microscope image (**Figure 2.5 (A)**) when the spin speed is lower. The spin coating speed can influence the coating condition. With higher spin speed, the coating can be more disperse. Whereas, a lower spin speed can make a more collective coating condition.

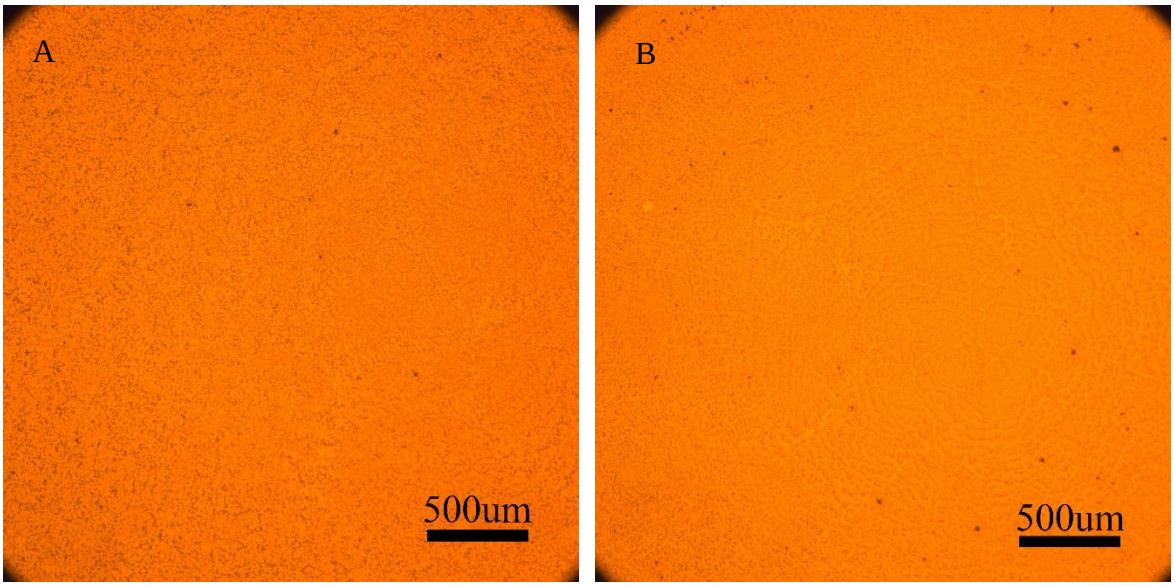

Figure 2.5 5x different spin speed of chloroform solution with 2.5mg toner (A: Spin speed of 2000RPM & B: Spin speed of 3000RPM)

Based on the experimental result above, the amount of solution placed on the coating substrate would not affect the coating condition during spin coating. With a certain coating solution, the coating condition is only related to the spin speed. With higher spin speed, the coating material obtains higher energy and velocity and can be thrown off and the coating would be thinner, which makes the dye particles distribute more evenly. On the other hand, with lower revolution speed, there is not enough energy and velocity for the

coating material to be spread out, thus, the coating is thicker, and the dye particles in the microscopic image distribute more densely.

2.4.1.2 Spin coating condition based on resin colorant

Since carbon nanopowder was not applicable as coating solution, resin colorant was attempted as a laser dye in the coating solution. 2.5mg colorant 75mg PS was applied in the solution with 1ml different solvents including DMF, chloroform, and toluene. After spin coating, there are dark shadows and spots distributed in the microscopic image as well (**Figure 2.6**). However, the resin colorant can have better solubility in solvents including DMF and toluene but performs worse in solvent including chloroform.

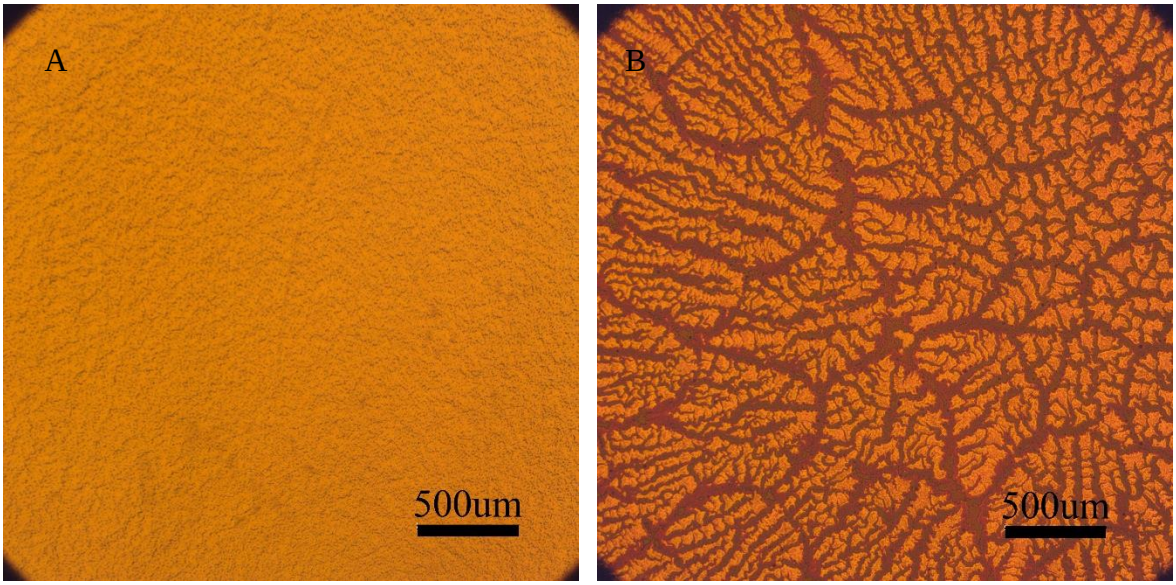

Figure 2.6 5x solution with 2.5mg colorant with different solvents
(A: DMF as solvent & B: Chloroform as solvent)

2.4.1.3 Spin coating condition based on IR165

After attempting carbon toner and resin colorant, IR165 was selected as another laser absorbing dye. Based on its solubility, chloroform was the common alternative solvent for both IR165 and PS. The chloroform solution with 2.5mg IR165 and 75mg PS was spin coated on the cover slip and amplified for 50 times, which is showed in **Figure**

2.7 (A). From the microscopic image, there is no dark shadow or black particles. However, numerous transparent bubbles are distributed in the coating. The amount of the dye in the solution was changed to investigate the effect of the dye concentration. The microscopic images of the coating condition of 5mg and 7.5mg IR165 were presented in **Figure 2.7 (B & C)**, respectively. The amount of bubbles is approximately same for solutions with different dye concentration, which excludes the effect of the dye concentration.

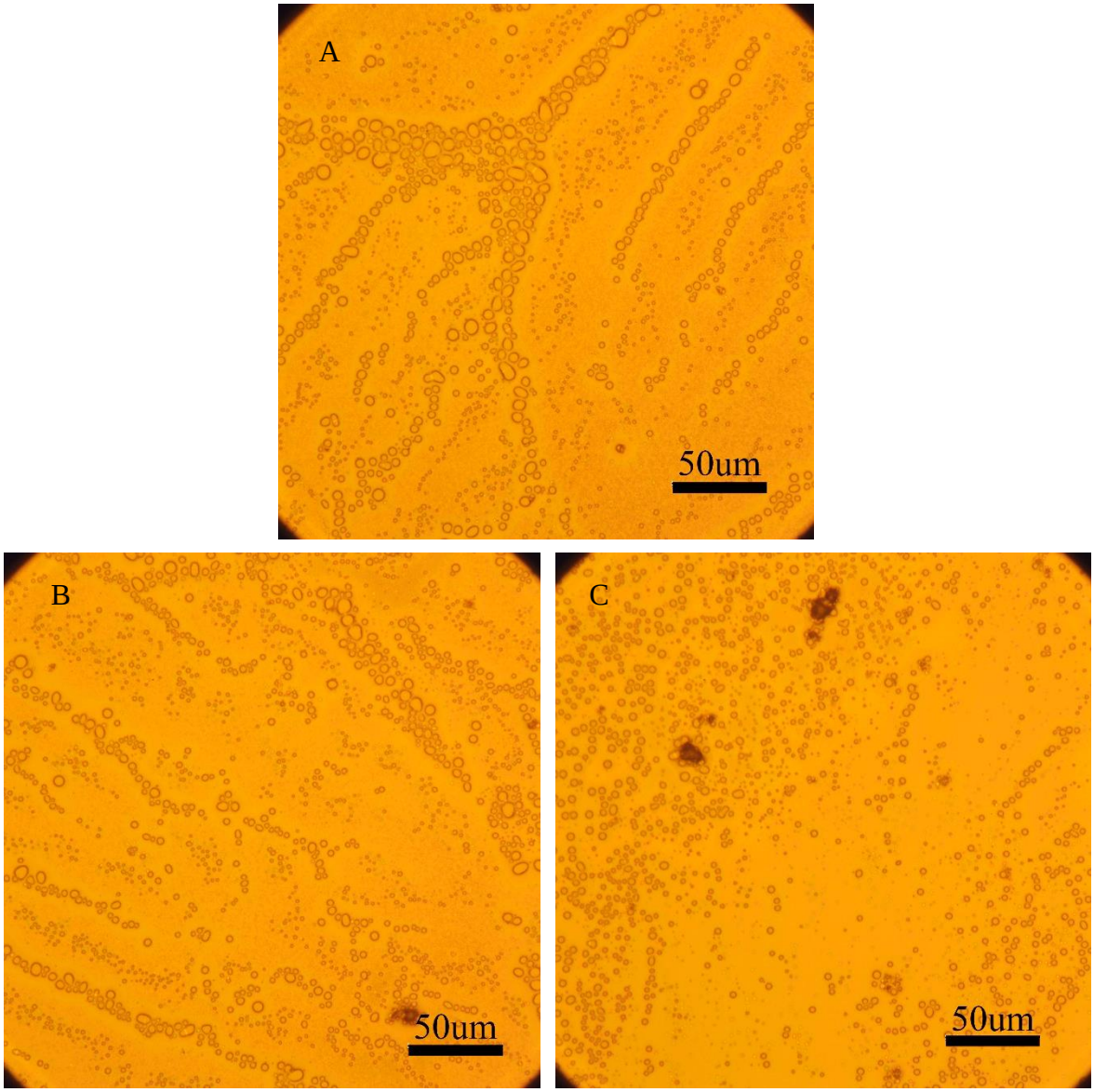

Figure 2.7 50x chloroform solution with various amount of IR165
(A: 2.5mg IR165, B: 5mg IR165 & C: 7.5mg IR165)

Considering the solutes may not be dissolved completely, another sonication was applied to the solutions above. The 50 times' microscopic images show a similar result to the coating condition at the first sonication (**Figure 2.8**), which means the solubilities of the solutes did not cause the formation of the transparent bubbles in the coating.

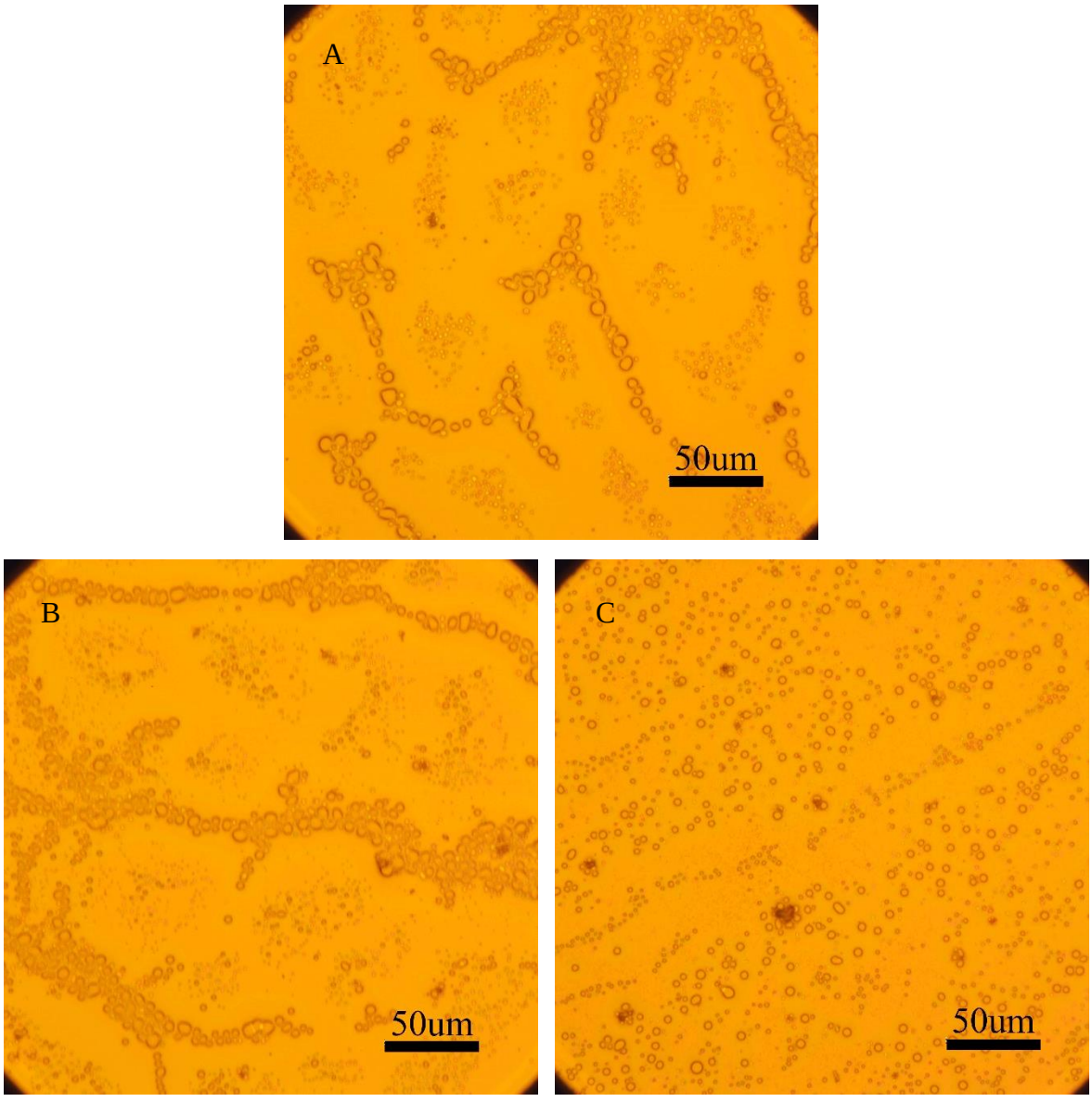

Figure 2.8 50x chloroform solution with various amount of IR165 after second sonicating (A: 2.5mg IR165, B: 5mg IR165 & C: 7.5mg IR165)

After excluding the effect of solutes, the reason for the transparent bubbles forming could be due to the solvent rapid evaporating while coating. Another organic solvent with a slower evaporation rate and good solubility for IR165 was found, which was cyclopentanone. The solution of 7.5mg IR165, 75mg PS, and 1ml cyclopentanone was sonicated for 20mins and spin coated on the cover slip at a revolution speed of 2000RPM. The 50 times' microscopic image of the coated glass substrate (**Figure 2.9**) displayed a completely transparent and uniform coating condition, which makes the composition acceptable as the coating solution which can produce consistent coating layer.

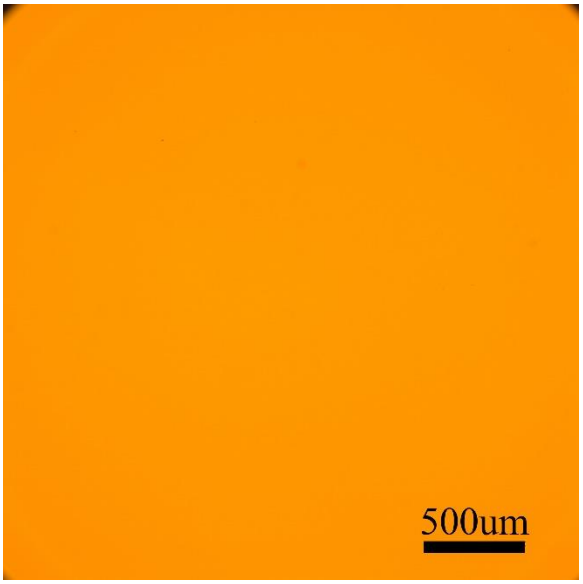

Figure 2.9 50x cyclopentanone solution with 7.5mg IR165 & 75mg PS

2.4.2 Verification of coating performance based on laser-induced ablation

The consistency of the coating was verified by creating a transparent and uniform coating layer on a spin coated cover slip. The laser-induced ablation was conducted on the cover slip coated by the coating material in order to certify the function of the laser dye and polymer. After three times of ablation, the ablation image (**Figure 2.10**) shown three distinct traces which are created by vaporizing the coated polymer on the glass substrate. These ablation traces can certificate the feasibility of the coating materials. The IR165 can

absorb the energy from a laser pulse and the absorbed energy can evaporate the PS. Moreover, the diameters of the ablation traces are 60.287um, 59.168um, 60.767um, respectively, which have approximate values to each other. The trace diameter is related to laser energy and coating properties only. Thus, with the consistent trace diameter at specific laser energy, a consistent ablation can be created based on the coating materials, which mean a consistent amount of polymer was vaporized in the ablation process. Therefore, the cavitation bubble has a high possibility to be consistently generated based on these coating materials in the laser-induced cavitation process.

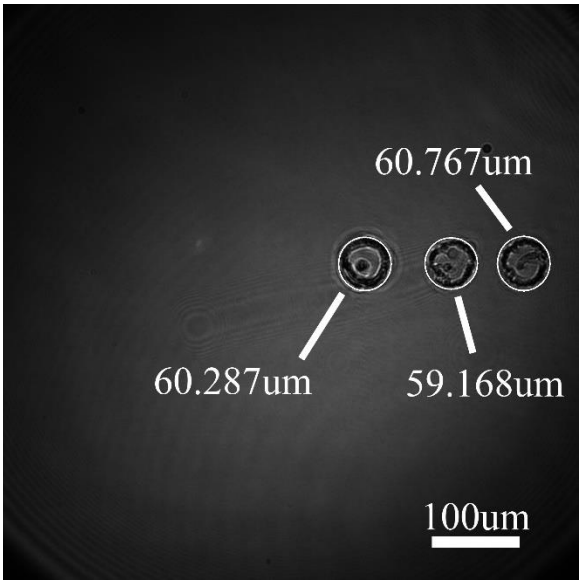

Figure 2.10 Top view of the ablation on coated glass

2.4.3 Certification of coating condition

To analyze the coating thickness with profilometer, a scratch was created on the coating layer by tweezers, where the surface of the glass substrate was appeared on the scratch (**Figure 2.11 (A)**). The coating around the scratched part from the solutions of 9%, 16.4%, 23%, 33%, and 50% PS spin coated at 2000RPM, 4000RPM and 6000RPM spin speed was 3D optically scanned by the profilometer, which was based on white light interference. The scanned result was recorded as the data of x-y-z coordinate values, which

can be plotted and reproduced by MATLAB. As an example, the 3D MATLAB plot is showed in **Figure 2.11 (B)**. The height values can be selected from the even part of the

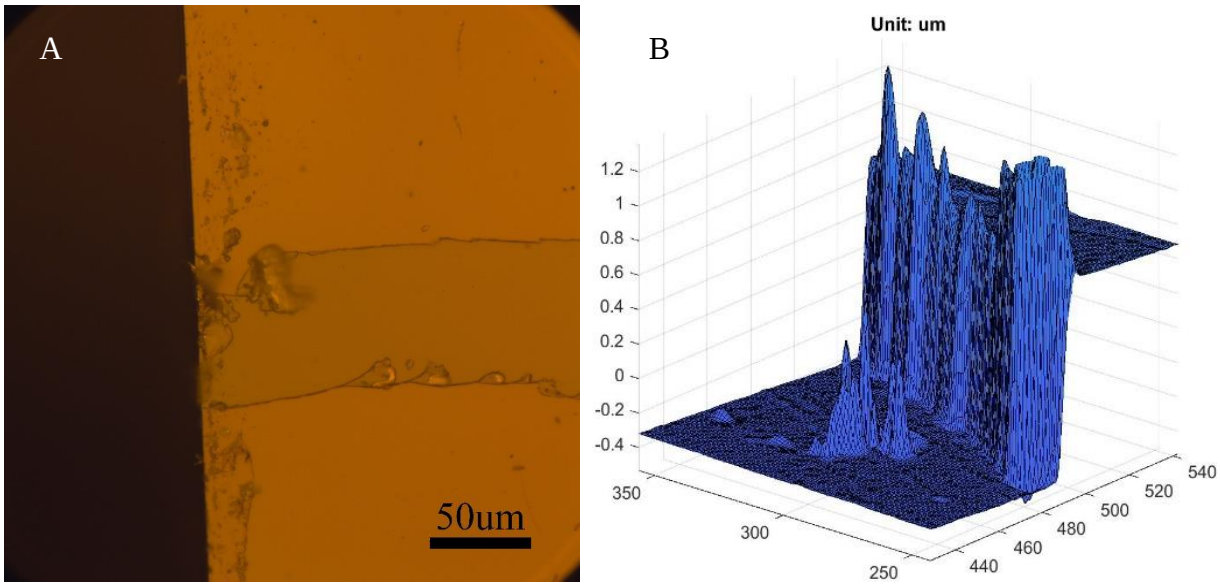

Figure 2.11 Solution of 23% PS spin coated at 2000RPM (A: 50x microscopic image of the scratch on coating & B: MATLAB plot of the scratch edge)

bottom surface and top surface in the plot to calculate the height difference of these two surfaces which is the thickness of the coating. Three points are randomly selected from both surfaces to improve the accuracy. The height difference from the substrate surface to the coating surface were calculated based on the average values of these three selected points from each surface. The data of the coating conditions at different spin speed, and PS concentration, including the height value of bottom and top surfaces and the coating thickness are listed in the table from **Table 2.1** to **Table 2.5**.

Table 2.1 Coating condition (um) of 9% PS solution at different spin speed (RPM)

	2000RPM			4000RPM			6000RPM		
	Upper	Lower	Thickness	Upper	Lower	Thickness	Upper	Lower	Thickness
1	0.2688	-0.06867	0.33747	0.1558	-0.08803	0.24383	0.05064	-0.08453	0.13517
2	0.2656	-0.06846	0.33406	0.1564	-0.08869	0.24509	0.05387	-0.08585	0.13972
3	0.2621	-0.06506	0.32716	0.1541	-0.08815	0.24225	0.04985	-0.08516	0.13501
Avg.	0.2655	-0.0674	0.3329	0.1554	-0.08829	0.24372	0.051453	-0.08518	0.13663

Table 2.2 Coating condition (um) of 16.4% PS solution at different spin speed (RPM)

	2000RPM			4000RPM			6000RPM		
	Upper	Lower	Thickness	Upper	Lower	Thickness	Upper	Lower	Thickness
1	0.2853	-0.5022	0.7875	0.1765	-0.3196	0.4961	0.2877	-0.1067	0.3944
2	0.2832	-0.5017	0.7849	0.1762	-0.3174	0.4936	0.2896	-0.1157	0.4053
3	0.2861	-0.4985	0.7846	0.1768	-0.3267	0.5035	0.2757	-0.0982	0.3739
Avg.	0.2849	-0.5008	0.7857	0.1765	-0.3212	0.4977	0.2843	-0.1069	0.3912

Table 2.3 Coating condition (um) of 23% PS solution at different spin speed (RPM)

	2000RPM			4000RPM			6000RPM		
	Upper	Lower	Thickness	Upper	Lower	Thickness	Upper	Lower	Thickness
1	0.2688	-0.06867	0.33747	0.1558	-0.08803	0.24383	0.05064	-0.08453	0.13517
2	0.2656	-0.06846	0.33406	0.1564	-0.08869	0.24509	0.05387	-0.08585	0.13972
3	0.2621	-0.06506	0.32716	0.1541	-0.08815	0.24225	0.04985	-0.08516	0.13501
Avg.	0.2655	-0.0674	0.3329	0.1554	-0.08829	0.24372	0.051453	-0.08518	0.13663

Table 2.4 Coating condition (um) of 33% PS solution at different spin speed (RPM)

	2000RPM			4000RPM			6000RPM		
	Upper	Lower	Thickness	Upper	Lower	Thickness	Upper	Lower	Thickness
1	0.2688	-0.06867	0.33747	0.1558	-0.08803	0.24383	0.05064	-0.08453	0.13517
2	0.2656	-0.06846	0.33406	0.1564	-0.08869	0.24509	0.05387	-0.08585	0.13972
3	0.2621	-0.06506	0.32716	0.1541	-0.08815	0.24225	0.04985	-0.08516	0.13501
Avg.	0.2655	-0.0674	0.3329	0.1554	-0.08829	0.24372	0.051453	-0.08518	0.13663

Table 2.5 Coating condition (um) of 50% PS solution at different spin speed (RPM)

	2000RPM			4000RPM			6000RPM		
	Upper	Lower	Thickness	Upper	Lower	Thickness	Upper	Lower	Thickness
1	0.2688	-0.06867	0.33747	0.1558	-0.08803	0.24383	0.05064	-0.08453	0.13517
2	0.2656	-0.06846	0.33406	0.1564	-0.08869	0.24509	0.05387	-0.08585	0.13972
3	0.2621	-0.06506	0.32716	0.1541	-0.08815	0.24225	0.04985	-0.08516	0.13501
Avg.	0.2655	-0.0674	0.3329	0.1554	-0.08829	0.24372	0.051453	-0.08518	0.13663

Based on the data from the tables above, the coating thickness and PS concentration curve at specific spin speed, and the coating thickness and spin speed curve at certain PS concentration can be plotted. The plots are presented in **Figure 2.12**.

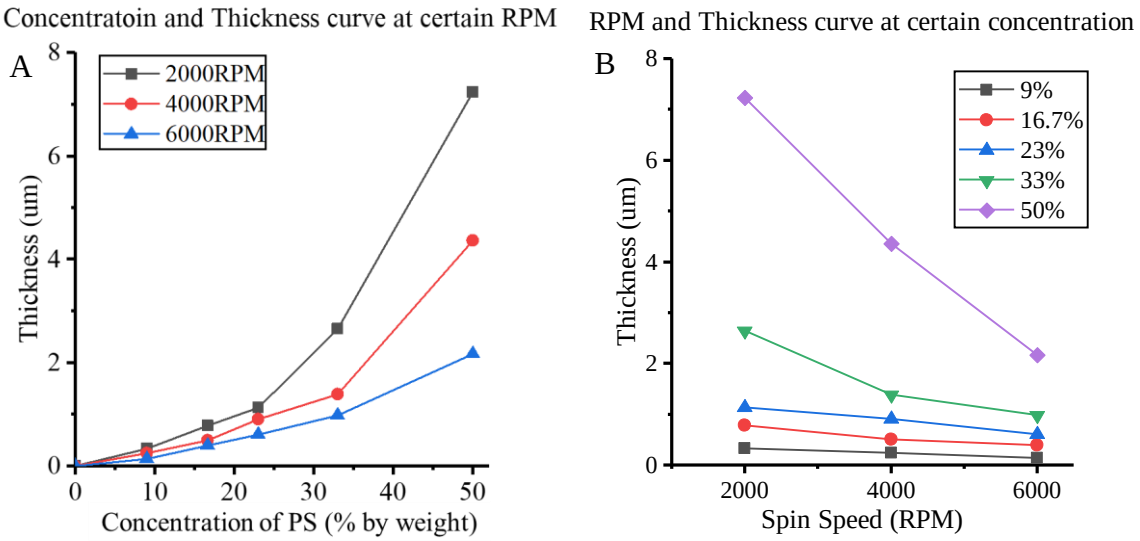

Figure 2.12 Coating thickness curves in different conditions (A: Concentration and thickness curve at certain RPM & B: Spin speed and thickness curve at certain concentration)

From the plots, the coating thickness nonlinearly and monotonically increases with the increasing of PS concentration at the same spin speed. Meanwhile, the coating thickness monotonically decreases as the spin speed increases at specific PS concentration. Additionally, at the same spin speed, the growth rate increases when the PS concentration is higher. The curve with lower spin speed has a higher growth rate, especially at higher PS concentration.

In the optical-fiber case, the spin coating on the end of the fiber is tough because of the construction of the optical-fiber which has considerable body length and tiny diameter. Thus, dip-coating can be applied to coat the solution on the fiber end. Based on the concentration and thickness curve, and the spin speed and thickness curve, the coating

should have a greater thickness as the PS concentration of the solution increases. However, the spin speed is 0RPM in the dip-coating; hence, the concentration and thickness curve for dip-coating should have a much larger increasing rate than the coating with spin speed. The thicknesses from solutions of all PS concentrations should be much larger than the coating thickness by spin coating. However, the coating thickness is not only related to the coating method and coating materials but the shape and material of the substrate can also affect it as well. Thus, the coating condition of the optical-fiber's dip-coating can only be simulated and speculated from the spin coating result. The precise status cannot be determined based on the spin coating condition.

2.5 Conclusions

To find the appropriate composition of the coating material for optical-fiber based laser-induced cavitation, the laser absorbing dye, evaporating polymer and a common organic solvent were tested. The objective was to find an integrated solution to create transparent and uniform coating layers, not only on spin coated cover slips but also on dip coated optical-fiber ends. Polystyrene was determined as the evaporating polymer because of its properties. In the experiment, carbon nanopowder, resin colorant, and IR165 were all considered as a laser absorbing dye. Carbon toner and resin colorant cannot create uniform coating with any alternative solvents like DMF, IPA, ethanol, toluene, chloroform and acetone. Black particles and dark shadows were remained on the coating after the solvent drying out. IR165 was completely dissolved in the organic solvent, chloroform. However, numerous of transparent bubbles appeared in the coating layer, which verified the rapidly evaporating solvent resulted in this. After choosing cyclopentanone as the organic solvent, the microscopic image of the coating materials' spin coated cover slip showed a completely

transparent and uniform coating layer, which certified the solution of IR165, PS and cyclopentanone as the final coating solution for the optical-fiber based laser-induced cavitation.

After selecting the coating solution's composition, the coating condition was investigated to find the relationship between the coating thickness and spin coating speed, as well as, coating thickness and PS concentration in the solution. With the plots of the relationships, when the other factors remained certain, the coating thickness grew as PS concentration increases, as spin speed decreases. The coating condition of optical-fiber's dip-coating can be speculated based on the conclusion from the spin coating. Same as the spin coating, the coating thickness should increase with the increasing of PS concentration. Since there is no spin coating in the dip-coating method, the spin speed for dip-coating is 0RPM. The coating thickness should be much greater than the coating by spin coating with the same PS concentration's solution.

CHAPTER 3

DEVELOPMENT OF THE OPTICAL-FIBER BASED LASER-INDUCED CAVITATION

3.1 Abstract

To set up the optical-fiber based laser-induced cavitation system, the optical-fiber is utilized to both propagate the laser pulse and conduct cavitation on the end surface which was aligned in the laser path of the previous LIC system. The end surfaces of the optical-fiber were polished by gradually smoother lapping sheets to achieve the functions consistently. The power calibration was conducted to certify the power input to and output from the fiber. These are used to verify the power loss of the propagation in the optical-fiber. Meanwhile, the fiber was aligned to reduce power loss and obtain the maximum power output based on the power calibration results. The cyclopentanone coating solutions of 50% PS, 0.375% and 0.75% IR165 were coated on the fiber end, which is then applied to conduct LIC in the water and gelatin sample. The cavitation behavior was studied based on expanding speed calculated from the multiple exposure images. In the water sample studies, the initial shooting time (T1) and subsequent shooting interval (T2) was varied to follow the expanding process. Though, the cavitation is inconsistent, the cavity magnitude and expanding speed vary because of the inconsistency of the coating thickness and input laser energy. The concentration of dye was changed to investigate the effect by the dye amount to the cavitation behavior. The expanding speed is more significant when the fiber is coated with a solution consistent with a higher amount of laser dye concentration. The absorbed laser energy increases when there is more dye contained in the coating layer, which accelerates the expanding process. The mechanical properties change when the 10%

gelatin sample replaced the water sample. To achieve the expanding speed in the water sample, the cavitation required more laser energy in the gelatin sample. Hence, the cavitation performs differently in the material with different mechanical properties, which makes this strategy possible to characterize high-strain-rate soft materials mechanically.

3.2 Introduction

According to the statistics of traffic collisions from the World Health Organization (WHO) by 2018, there have been tens of millions more traffic crashes occurring throughout the world and six million of these accidents happen in the United States every year. Moreover, there are an estimated 39,888 people who died in the traffic collisions in the US in 2016, which is nearly 110 people dying every day(World Health Organization, 2018). Among them, there are approximately 10,656 fatalities related to traumatic brain injury (Alexis B. Peterson, 2019). Additionally, 58,765 people are hospitalized because of traumatic brain injury due to these traffic accidents. However, traffic collisions are only the second leading reason of the traumatic brain injury related hospitalization which is 20% from all the reasons for traumatic brain injury-related hospitalization (Centers for Disease Control and Prevention, 2019).

Hence, it is necessary and critical to study the brain properties, including the mechanical properties. Laser-induced cavitation system can mechanically characterize high-strain-rate soft materials, including brain tissue based on the cavitation behavior in the investigated target. Our research group has developed this approach by introducing laser absorbing seeds to develop the LIC by improving the feasibility and consistency. With improvement, cavitation can be generated with significantly lower laser energy because of the laser dye particles spread all around the seed particle. Meanwhile, the consistency can

be guaranteed in different samples with the polymer particle located in the center, which is used to vaporize to form a cavity in the sample. However, the seed particles placed on the surface of the established samples cannot conduct cavitation in the interior of the sample. Furthermore, even if the particles are blended previously in the sample, the laser energy delivered to the cavitation spot can be influenced if the sample is not entirely transparent, especially, in the brain tissue which floats cells and other substance in the tissue (**Figure 3.1**). The laser properties may change as it is passing through the brain tissue. An optical-fiber that can be inserted into the samples was employed to both propagate laser pulse and conduct cavitation on the end surface. The laser will be delivered to the inside of the sample and will directly generate cavitation on the end surface of the fiber, without passing through the tissue. The effect of the opaque sample was excluded from the cooperation of the optical-fiber. In this study, the approach was developed by conducting cavitation in different samples with coating materials of varying dye concentrations.

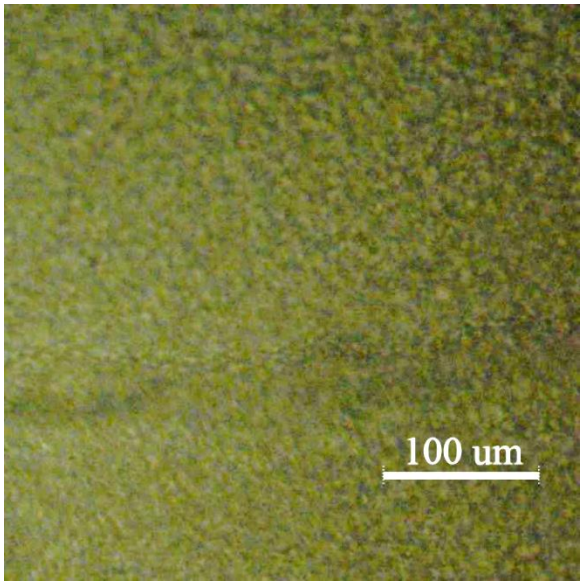

Figure 3.1 Rat brain tissue under 2.5 times zooming-in

3.3 Materials and Method

3.3.1 Preparation of the coating solution

2ml cyclopentanone was dropped by a 10-100 microliter pipette (Sci Logex). 2g polystyrene weighed by the analytical balance (Mettler Toledo) was added into the solvent to prepare the solution of 50% PS concentration. The IR165 (Luxottica Exciton) which is an inferred absorber was weighed for 0.015g and 0.03g by an analytical balance (Mettler Toledo) and added into the solution for preparation of 0.375% and 0.75% dye concentration respectively. The solution was blended by a sonicator (Branson 1510) for 20 min, after which the dye and polymer were completely dissolved in the solvent. Therefore, the coating solution of 50% PS with 0.375% dye, and the coating solution of 50% PS with 0.75% dye was prepared for the cavitation.

3.3.2 Preparation of samples

The cavitation was conducted in the testing samples to develop the optical-fiber based LIC system. In the experiments, distilled water and 10% of gelatin were employed as testing samples to study cavitation behavior and investigate cavitation in samples with different concentrations.

3.3.2.1 Preparation of water sample

A container was required to contain a sample to conduct cavitation in the water sample. This can be observed under a microscope and inserted by optical-fiber (ThorLabs) to perform cavitation in the sample. The sample container was made by sticking three of the cover slip's sides (Fisherbrand^{TM}, 25mm x 25mm) on the center of the microscope slide (Fisherbrand^{TM}, 25mm x 75mm x 1.0mm) with hot melt glue, the interval from the microscope slide to the cover slip was approximate 1mm. The glass slides were both rinsed

with water and soap water and dried with the high-pressure gas flow. Then, the water sample was produced by inserting the distilled water into the sample container with a glass pipette (**Figure 3.2**).

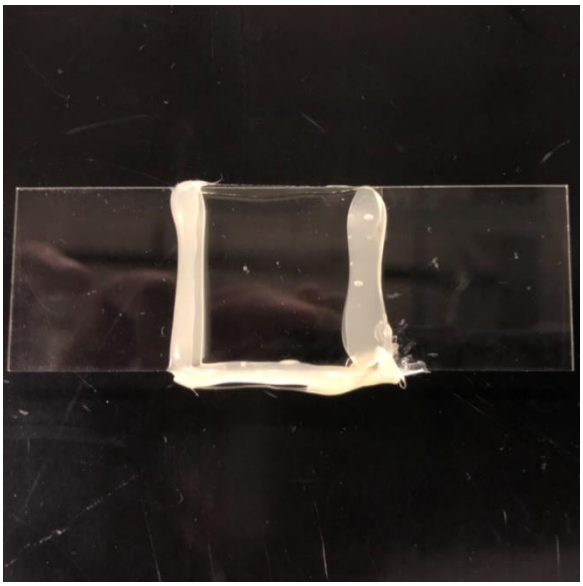

Figure 3.2 Distilled water sample

3.3.2.2 Preparation of gelatin sample

The gelatin sample with 10% concentration by weight was prepared with 0.5g gelatin powder (from porcine skin, gel strength 300, Type A, Sigma-Aldrich) was weighted by analytical balance (Mettler Toledo) and placed in a with lid glass tube. A graduated glass pipette with glass filler was used to measure 4.5ml distilled water and inserted in the glass tube containing gelatin powder. A magnetic stirring bar was placed in the mixture and heated the isotemp stirring hotplate (11-300-49SHP, Fisher Scientific) to 100 ° C. Then, the glass tube, which contains the mixture, was placed on the heated hotplate, and the stirring function was applied to the hotplate at 200RPM. The mixture was stirred on the hotplate until the gelatin powder completely dissolved in water. After cooling down, the 10% gelatin gel was inserted into and filled the sample container. Then the sample was refrigerated for at least 90 min to solidify the sample.

3.3.3 Power calibration

As showed in **Figure 1.6**, the optical-fiber consists of a protective layer, cladding, and core. The ablation laser is focused into the core of the optical-fiber and propagates within the core as it is reflected off the cladding. Thus, the laser would not lose energy while propagating in the fiber. However, to deliver the laser pulse in optical-fiber, the laser has to be incident on the core, which is only tens of microns. Hence, the alignment between the laser pulse and fiber core is challenging. Additionally, the flatness of the fiber's end surfaces is important to reduce power loss.

The optical-fiber was polished with gradually smoother lapping sheets to ensure the flatness of the end surfaces. After peeling off the protective layer around the fiber end, the optical-fiber was fixed by a fiber holder (BFT1, Thorlabs) which is screwed into a mental optical-fiber polishing disc (D50-SMA, Thorlabs). The end surface is on the same plane as the bottom surface of the polishing disc. Then the fiber was polished on the 5um, 3um, 1um's aluminum oxide lapping sheet and 0.3um's calcined alumina lapping sheet (Thorlabs) which are placed on a frosted glass by drawing 8-shaped as the lapping sheets are sprayed by water. After polishing, the fiber is rinsed by IPA and water and observed under the stereomicroscope (SZX7, Olympus) to verify the flatness of the end surface.

After polishing, the fiber was installed in the LIC. The Nd:YAG pulsed laser (Quanta-Ray INDI-40-10-HG, Spectra-Physics) was employed to provide an ablation laser (10Hz). A green laser which shares the same optical path with the ablation laser is applied to adjust the alignment visually. The optical-fiber that is on the optical path of the ablation laser should also be on the optical path of the green laser. Thus, the green laser should be visible from the output end of the optical-fiber. By changing the position of the input end

of the optical-fiber to find the brightest output green laser with the fixing screws, the optical-fiber is preliminarily aligned in the optical path, qualitatively. Then, a power meter (Model 1918-R, Newport) was employed to quantitatively measure the accurate energy on both the input and output ends of the optical-fiber. The Nd:YAG laser was triggered at specific power and external mode when the energies on both ends of the fiber were measured. As the energy is measured on the output end, the position of the input end was adjusted furthermore to achieve the most significant output energy based on the reading on the power meter. The energies on both ends were recorded, and the energy loss was calculated according to:

Energy loss = (Energy input – Energy output) / Energy input

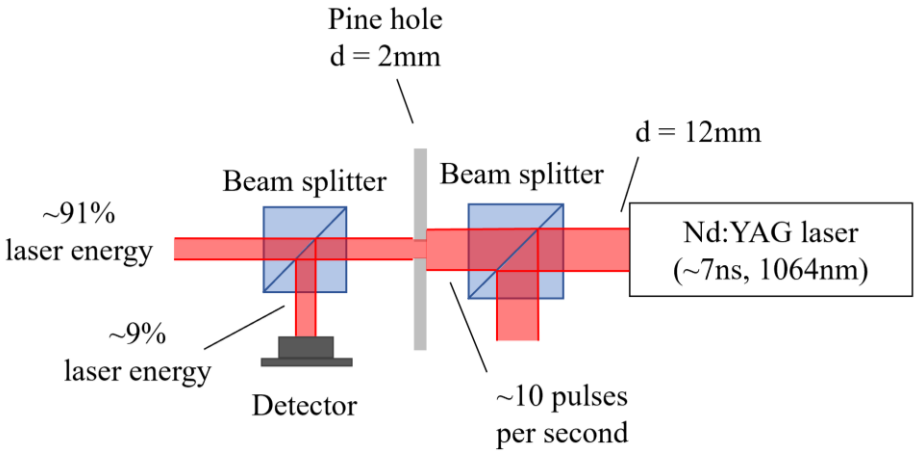

Figure 3.3 Construction of the ablation laser emission part

Additionally, as showed in **Figure 3.3**, the ablation laser pulse initially emitted from the Nd:YAG laser with the diameter of 12mm was partially blocked by a beam splitter. The output of laser energy can be controlled by rotating the beam splitter. A pine hole with the diameter of 2mm was employed to reduce the laser energy. The reduced laser beam was split by a beam splitter and delivered ~9% of the laser beam to a detector to measure the energy of the partial laser beam. The other ~91% laser energy was applied for the cavitation experiment.

3.3.4 Coating and dissolution of the laser absorbing film

Since the optical-fiber is exceptionally slender with minimal diameter and great length, spin coating is unlikely to be applied to add coating solution to the fiber end. Thus, dip-coating was employed instead of spin coating. The output end of the fiber, around which the protective layer has already been peeled off, was immersed into the coating solution head down and pulled out to air dry head down for a several minutes. Meanwhile, the coating thickness on the end surface of different coating solutions that are 50% PS, 60% PS and 66.7% PS respectively with 0.0375% IR165 were measured based on microscope and measurement software.

After cavitation, if there is polymer remaining on the fiber, this will affect the future cavitation. Thus, the coating needs to be removed to conduct the second cavitation. The coating part of the fiber was initially rinsed with acetone and wiped with a piece of nonwoven wipers (TX609 Texwipe) which was immersed in acetone. To certify that the coating has been removed, the coated part was laso immersed into acetone for a few seconds. The fiber can be dip coated again after cleaning and a second cavitation can be created.

3.3.5 Investigation of optical-fiber based LIC

After alignment, the coated optical-fiber, held by a fiber holder, was inserted into the sample in the sample container and placed on the sample stage. The stroboscopic image laser (pulse duration ~100fs, wavelength ~780nm, repetition rate ~80MHz) which was provided by a Ti:Sapphire oscillator (Mai-Tai HP, Spectra-physics) was employed to illuminate the interface from the optical-fiber to the sample. The cavitation event happed on the interface was recorded by the target camera with amplification from 0-2.5 times as

multiple exposure image (**Figure 3.4**). The first illumination pulse was emitted after the emission of the ablation laser pulse; the interval between these two pulses is recorded as T1. The delay time between the contiguous illumination pulses after the first pulse was recorded as T2. In the multiple exposure image of the cavitation process, the expanding

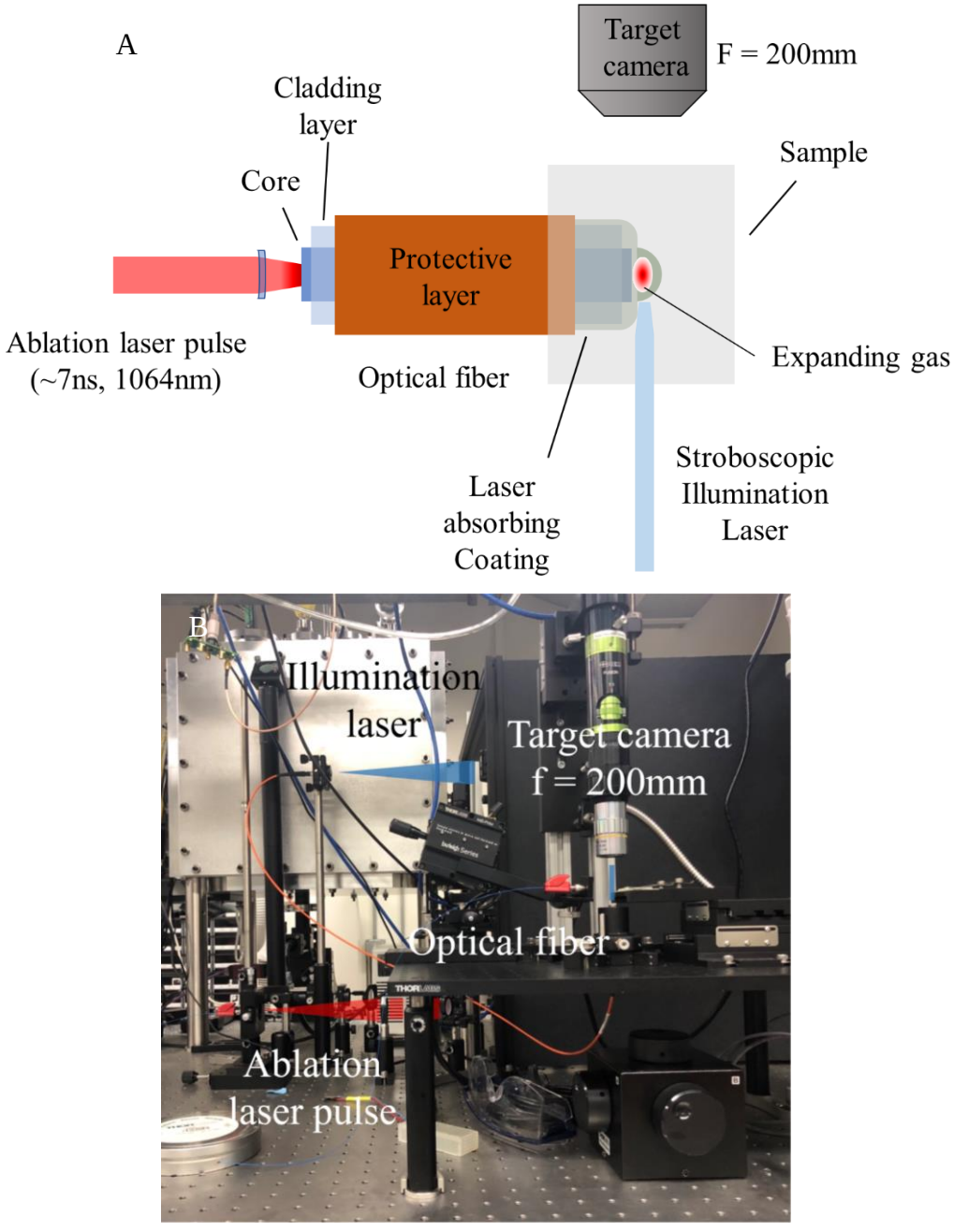

Figure 3.4 Construction of optical-fiber based LIC (A: Schematic diagram of construction & B: Photograph of construction)

event was recorded as bubbles in different radius at the corresponding time. The dynamic blur can be excluded due to the duration of the illumination pulse which is only ~100fs. The perpendicular line segment from the middle of the fiber's end surface to the bubble surface which is perpendicular to the end surface was counted as the radius of the bubble. The expanding velocity can be calculated based on $v(t1) = \frac{r2 - r1}{t2 - t1}$, where t1 = T1, t2 = T1 + T2, r1 and r2 are the radii of the first and second bubbles counted from the center.

3.4 Results and Discussion

3.4.1 Coating thickness on the optical-fiber end

With the microscope image of the fiber end, the length of the line segment from the end surface to the coating surface which is perpendicular to the end surface is the coating thickness (**Figure 3.5 A**). The measurement results of different coating solutions are plotted in **Figure 3.5 B**. For each solution, there are six measurements. From the plot, a solution with higher PS concentration can create a thicker coating. However, the dip-coating is not an entirely consistent coating method for optical-fiber; the coating thickness varies with different variation rate for a different solution. The variation rate increases as the PS concentration increases, which means the coating thickness has larger diversity created by solution with higher PS concentration. A fitting curve was plotted with an exponential growth model, $h(c) = a_0[\exp(c/c_0) - 1]$, where a_0 = 3.05 and c_0 = 18.70. Based on the measurement result and fitting curve, both the coating thickness and diversity were considered to select the optimal coating solution. The PS concentration should be duly high to make cavitation that has abundant expanding speed to be recorded by stroboscopic camera. The solution of 50% PS which can create an appropriate coating

thickness and have lower coating inconsistency was selected in the cavitation experiments for its higher thickness consistency and appropriate performance in cavitation experiment.

3.4.2 Results of laser power calibration

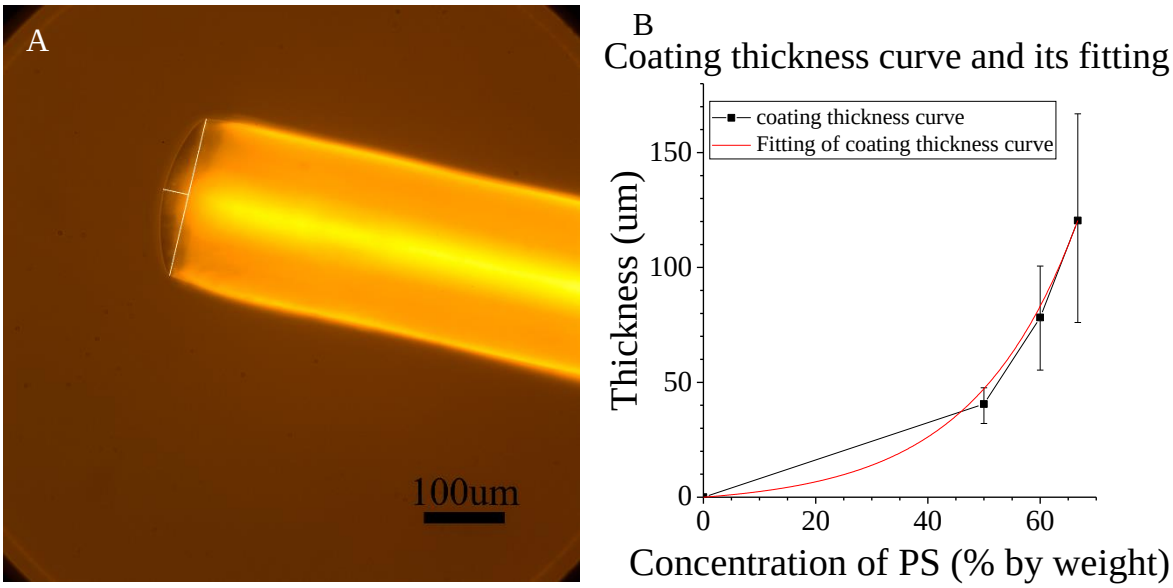

Figure 3.5 Coating on fiber end (A: Photograph of coated fiber & B: Plot of coating condition)

After power calibration, the output power from the fiber has achieved the optimal value. The calibration results at setting ablation laser pulse energy of 220uJ and 435uJ are shown in the tables (**Table 3.1** & **Table 3.2**).

The reference power was the environment optical power measured without ablation laser input. The power measured after triggering the ablation power was recorded as the input or output power. The final input or output power was calculated by subtracting the reference power from the input or output power. From the calibration results, the coupling efficiency between the optical-fiber and laser path were 3844.12 / 4659.513 ~= 82% and 4504.95 / 6108.213 ~= 74% at the setting energy of 220uJ and 435uJ, respectively. However, considering the inevitable laser reflecting from both end surfaces of the optical-

fiber, which is 4% + 4% = 8% reflected laser energy, the coupling efficiency is about 89% and 80%, respectively compared with the possible maximum coupling efficiency.

Table 3.1 Power calibration results at pulse energy of 220uJ

	Power Input (uW)			Power Output (uW)		
	ref.	power	power-ref.	ref.	power	power-ref.
1	18.45	4680	4661.55	-13.38	3830	3843.38
2	17.93	4710	4692.07	-13.74	3850	3863.74
3	15.08	4640	4624.92	-15.24	3810	3825.24
avg.	17.15333	4676.667	4659.513	-14.12	3830	3844.12

Table 3.2 Power calibration results at pulse energy of 435uJ

	Power Input (uW)			Power Output (uW)		
	ref.	power	power-ref.	ref.	power	power-ref.
1	-75	6080	6155	24.81	4630	4605.19
2	-64.8	6140	6204.8	77.61	4460	4482.39
3	-44.84	5920	5964.84	22.73	4450	4427.27
avg.	-61.5467	6046.667	6108.213	41.71667	4480	4504.95

3.4.3 Cavitation using distilled water sample

The cavitation was conducted in the water at the output laser power of approximate 3844uW. The coating solution of 50% PS and 0.0375% IR165 and solution of 50%PS and 0.075% IR165 were coated onto the fiber to investigate the cavitation behavior. The expanding process was recorded by multiple exposure images with different T1 and T2 values. In **Figure 3.6 A**, for example, T1 and T2 are 1000ns and 1269.5ns respectively. Thus, the radii of the bubbles are r1= 148.346um, r2 = 175.591um r3 = 200.77um and r4 = 218.933 which are captured at t1 = T1 = 1000ns, t2 = T1 + T2 = 2269.5ns, t3 = T1 + 2T2 = 3539ns and r4 = T1 + 3T2 = 4808.5ns, respectively. The cavitation behaviors are plotted in **Figure 3.6 B**, the radii of the cavities vary along with the delay time after the emission of the ablation laser. The cavitation conducted by a solution of 50% PS and 0.0375% IR165 is plotted as event 1-1 to 1-6. The event 2-1 and 2-2 are cavitation events conducted by a

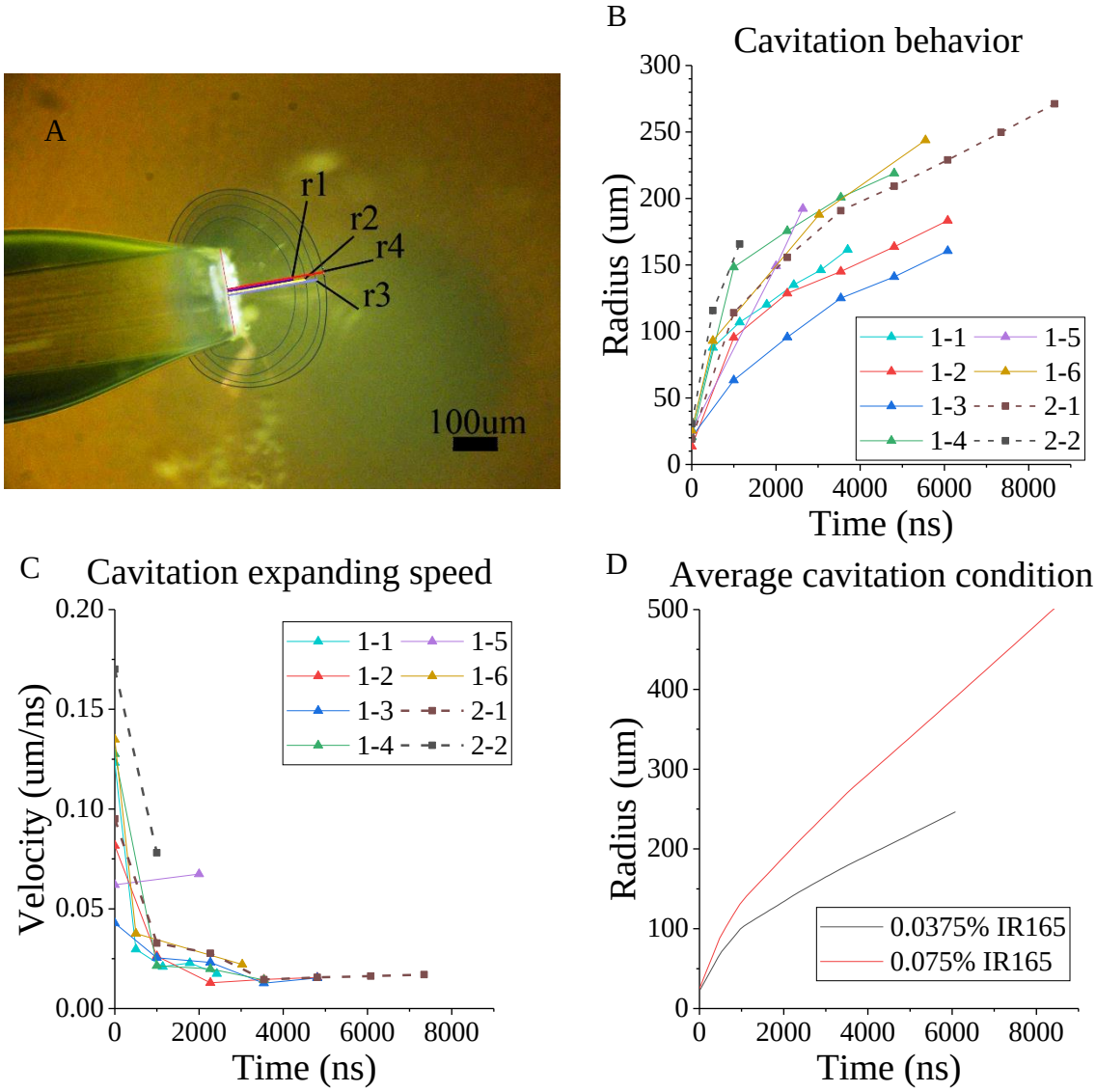

Figure 3.6 Cavitation behavior (A: The cavitation event at T1 = 1000ns and T2 = 1269.5ns, B: Cavity radius and time curve, C: Expanding speed and time curve & D: Mean curve of cavitation condition with different dye concentration)

solution of 50% PS and 0.075% IR165. The cavitation behaviors are conducted with the same laser power which is about 38844.12uW. Since the Nd:YAG laser is pulse laser, there is up to approximate 10uJ, 4.5%, fluctuation in the triggered ablation laser, which can lead to the variation in the output laser power. However, the different rate in the cavitation radius can be up to about 135% at the same time as 1000ns but in various cavitation events, event 1-3 and event 1-4. Hence, the fluctuation of the laser energy can only partially lead

to the variation of the cavitation behavior. Though the radii of the cavities fluctuate rapidly, the expanding curves are following similar trends. Combining with the expanding speed curves in **Figure 3.6 C**, the cavitation has higher but decreasing expanding speed at the initial stage before 3500ns. The expanding speed becomes steady after the initial stage and all the cavitation events tend to expand at approximately the same speed.

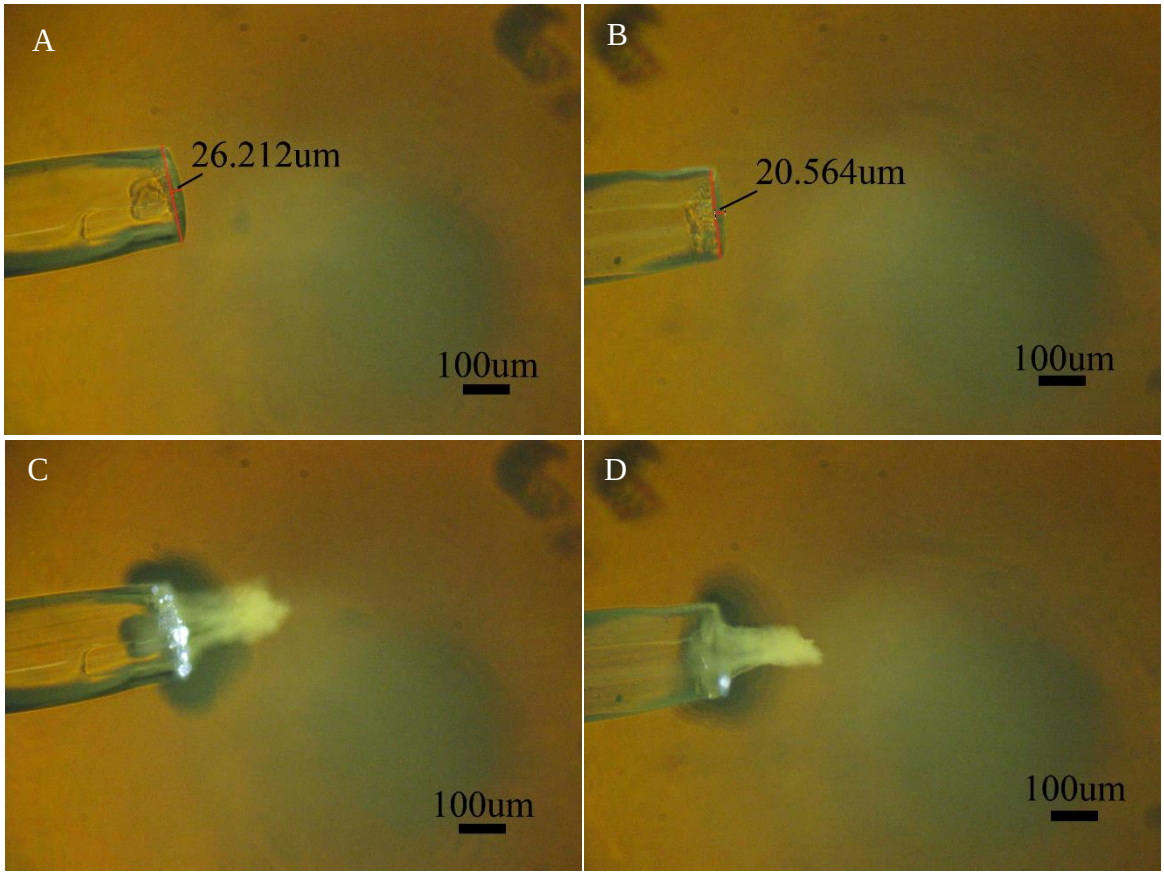

Figure 3.7 Coating condition and Cavitation behavior (A: Coating condition of event 1-1, B: Coating condition of event 1-3, C:Cavitation behavior for event 1-1 & D:Cavitation behavior for event 1-3)

Comparing event 1-1 with 1-3, cavitation in 1-1 has a larger radius at the same time spot and higher initial expanding speed. According to **Figure 3.7**, for event 1-1, the polymer coating is 26.212um which is thicker than 20.564, the thickness for event 1-3. The flashlight which can represent the energy absorbed by the coating is brighter for the cavitation event 1-1 than it for event 1-3. It can be inferred that the coating thickness on

the end surface can largely influence the initial cavitation radius; the radius can be larger with a thicker coating. The absorbed laser energy can affect the amount of evaporated polymer, which can both influence the initial bubble radius and expanding speed. Higher laser energy can vaporize more polymer. Thus, the initial cavity bubble can be more significant with higher subsequent expanding speed. Therefore, with thicker coating and higher laser energy, the cavitation 1-1 has a larger cavity and higher expanding speed than cavitation1-3. The other events plotted in **Figure 3.6 B&C** follow the same principles, event 1-1 has approximative strength of flashlight but much thicker coating compared to event 1-2. Hence, cavitation 1-1 has a higher initial expanding speed than 1-2's. However, the laser energy is not abundant to evaporate all the polymer coated on the fiber; the difference between the cavities' magnitude is not as significant as the difference between the coating thicknesses. Even though event 1-4 to event 1-6 have approximative coating thickness to event 1-1, the initial expanding speed and cavity magnitude are much larger than event 1-1's since the laser energies of event 1-4 to 1-6 are much higher than event 1-1's. Furthermore, for cavitation event 2-1 and 2-2, the concentration of laser absorbing dye in the coating is increased to twice amount than the coating for other cavitation events. Thus, a relatively higher expanding speed can be created than the event 1-1 to 1-3 with lower laser energy. However, due to the smaller coating thickness, event 2-1 has a lower initial expanding speed than event 1-4 and 1-6. Regardless of the thinner coating, the event 2-1 with higher laser energy has close cavity magnitude and expanding speed to event 1-4 to 1-6 which has a relatively thicker coating. The event 2-2 that has thicker coating can generate larger cavity with higher initial expanding speed. Furthermore, the mean curves of cavitation with different dye concentration in the **Figure 3.6 D** illustrate that the

cavitation conducted by higher dye concentration can have higher expanding speed and larger cavity size. However, with the inconsistency in coating thickness and laser energy, the coatings with higher dye concentration can still create cavitation with approximative behavior to the coating with lower dye concentration.

Additionally, the coating inconsistency was caused by the dip-coating process which created a coating layer with various coating thickness. Whereas, the energy inconsistency was conducted by the destruction of the optical-fiber (**Figure 3.8**). In the experiment, the ablation laser pulse was focused on the input end of the optical-fiber to reduce the energy loss, since the radius of the fiber core can be as small as few microns. The local energy is extremely high as the laser is highly focused on adapting the fiber core. Thus, the end surface of the laser input and middle part can be destroyed by the laser energy. Then, the input energy was reduced due to the structure destruction.

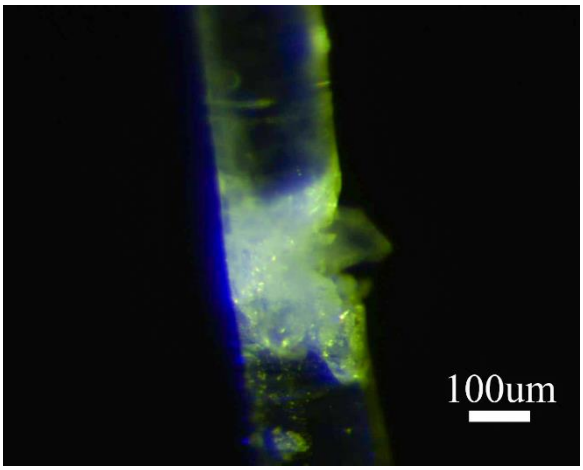

Figure 3.8 Destruction of the optical-fiber

3.4.4 Cavitation in gelatin sample

The cavitation was conducted in the 10% gelatin sample with a solution of 50% PS and 0.0375% IR165. Since the viscoelasticity of the gelatin sample is much higher than the water sample. Higher output laser power, 4504.95uw was employed to create cavity bubble in gelatin sample. Even with higher laser power, the cavities created in gelatin of event 1

and 2 are weaker than most cavitation in water (**Figure 3.9**). For cavitation events in gelatin, the initial radius at the first exposure time are close to 80um. Whereas, for six cavitation events in water, most of the initial radius at the first exposure time are close to 90um. However, the expanding speed is much higher than those in water sample, probably due to higher laser energy. In the mean curves, the cavitation in gelatin have approximative initial expanding speed to the cavitation in water with 0.0375% laser dye. However, the cavitation in latter stage have even higher expanding speed than in water with 0.0075% laser dye. Thus, the laser-induced cavitation can have different behaviors in different samples. The

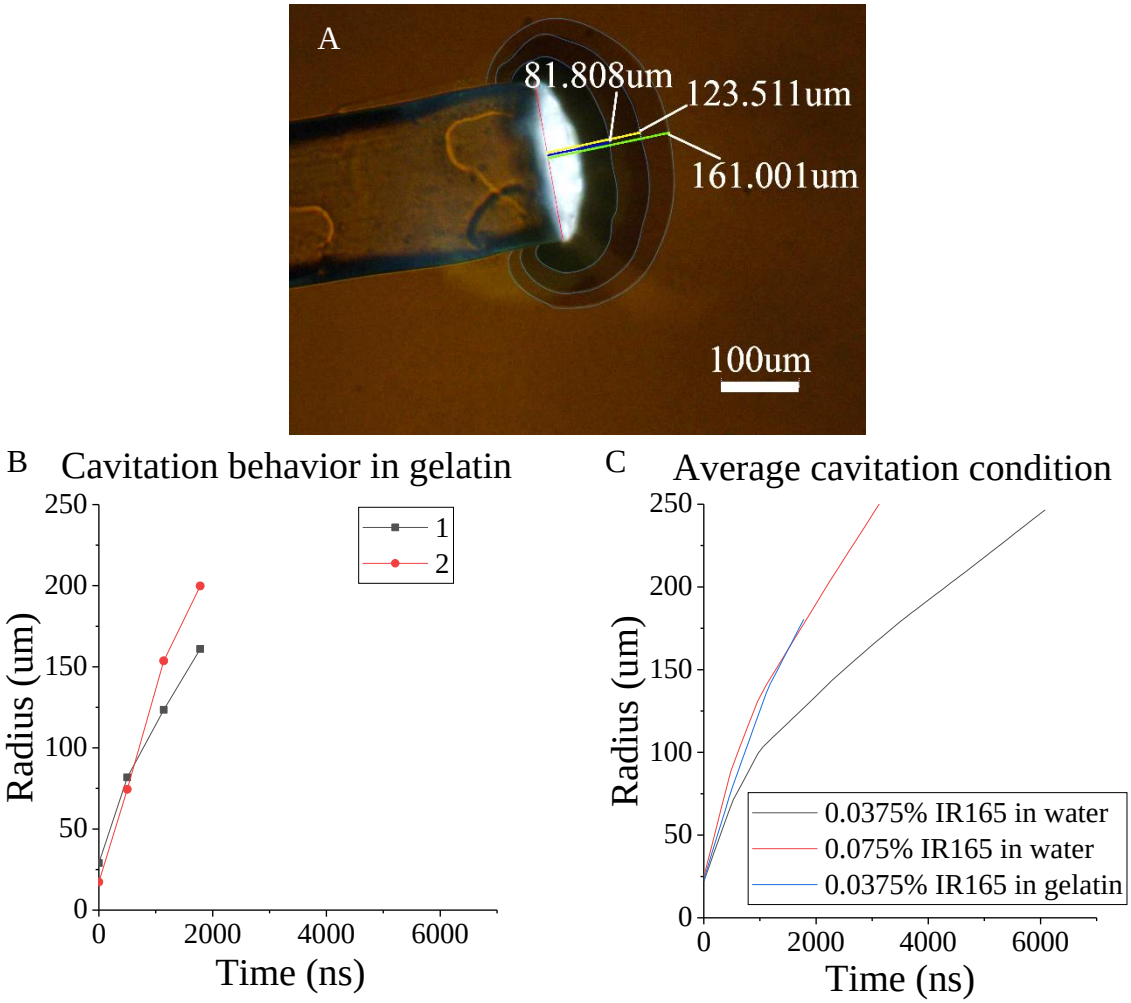

Figure 3.9 Cavitation in 10% gelatin sample (A: The cavitation event at T1 = 500ns and T2 = 641.03ns, B: Cavity radius and time curve & C: Mean curve of cavitation condition with different dye concentration in different samples)

cavitation in high-strain-rate soft material with higher viscoelasticity have relatively smaller initial cavity size than those in lower viscoelasticity's sample. Thus, with models of viscoelasticity, soft materials can be mechanically characterized based on the cavitation behavior in optical-fiber based laser-induced cavitation with initial and critical cavity magnitude and expanding speed.

3.5 Conclusions

Based on the coating measurement, the coating on the end of the optical-fiber can be thicker as the PS concentration in coating solution becomes higher. However, the coating thickness is inconsistent with the dip-coating method. While conducting cavitation in the water sample, the expanding speed was more elevated and decreasing in the initial stage before 3500ns. After that, the expanding speed became steady. Regardless the incomplete evaporation of the PS, the coating layer with higher laser dye concentration can create a cavity bubble with higher expanding speed as the coating thickness stays steady because higher laser energy can be absorbed by the coating with higher dye concentration. For the cavitation in 10% gelatin sample, the cavitation with 4504.95uW output laser power have even smaller magnitude but higher expanding speed than the cavity magnitude in water with 3844.12uW output laser power. Since, with higher viscoelasticity, the evaporated PS requires more energy to create same size of cavity bubble in gelatin that water. However, the much higher laser energy can still accelerate the expanding process after the initial process, even in the gelatin sample. But the cavitation behavior is irregular due to the inconsistent coating thickness and the input laser energy, which destroys the optical-fiber. The inferences cannot be verified entirely until the consistency of the system has been certificated.

3.6 Future work

To improve the consistency in the optical-fiber based laser-induced cavitation, the consistency of coating thickness and input laser energy will be improved, jointly. A coating method with higher consistency will be applied, the solution amount initially located on the end surface need to be stable. There should be no liquid exchange from the end surface to the side surface of the fiber. For example, the coating solution can be dropped by pipette onto the optical-fiber which is positioned head up and held steadily. The coating condition will be investigated to verify the consistency of the new coating method. To avoid the destruction on the input side end surface of the optical-fiber, an optical-fiber with a larger diameter can be employed to deliver the laser beam with a larger diameter and lower focusing. Besides, a lower laser energy can be applied to reduce the possibility of the destruction of the optical-fiber. To achieve the same cavitation condition with lower laser energy, the dye concentration in the coating layer can be increased to absorb the same energy from the laser with lower power.

After creating cavitation with consistent cavity magnitude and expanding speed, the mechanical model will be found and simulated with a gelatin sample to achieve the application of mechanical characterization on soft materials based on gelatin samples in different concentrations. With the mechanical model, the optical-fiber based laser-induced cavitation can be applied to mechanically characterize high-strain-rate soft materials with unknown mechanical properties, including rat brain tissue.

REFERENCES

A. G. Molchanov. 1970. Development of avalanche ionization in transparent dielectrics under action of a light pulse. SOVIET PHYSICS SOLID STATE, USSR. 12: 749.

Alexander S. Zibrov, Mikhail D. Lukin, Dmitri Evgenievich Nikonov *et al*. 1995. Experimental demonstration of laser oscillation without population inversion via quantum interference in Rb. 75: 1499-1502.

Alexis B. Peterson, Jill Daugherty, Matthew J. Breiding *et al*. 2019. Surveillance report of traumatic brain injury-related emergency department visits, hospitalizations, and deaths, United States.

Anna Bellini & Selçuk Güçeri. 2003. Mechanical characterization of parts fabricated using fused deposition modeling. Rapid Prototyping Journal. 9: 252-264.

Apostolos G. Doukas, Daniel J. McAuliffe & Thomas J. Flotte. 1993. Biological effects of laser-induced shock waves: Structural and functional cell damage in vitro. Ultrasound in Medicine & Biology. 19: 137-146.

B. Ward & D.C. Emmony. 1990. Conservation of energy in the oscillations of laser-induced cavitation bubbles. The Journal of the Acoustical Society of America. 88: 434-441.

Bartosz Kawa, Krzysztof Adamski, Danylo Lizanets, *et al*. Jun 2018. Mechanical characterization of inkjet 3D printed microcantilevers. : 1-3.

Centers for Disease Control and Prevention. 2019. Traumatic brain injury & concussion. 2019.

Christorpher Earls Brennen. 2014. Cavitation and Bubble Dynamics. Cambridge University Press.

Claus-Dieter Ohl, Manish Arora, Rory Dijkink *et al*. 2006. Surface cleaning from laser-induced cavitation bubbles. Applied physics letters. 89: 07410-3.

E. V. Sysoev, I. A. Vykhristyuk, R. V. Kulikov *et al*. 2010. Interference microscope-profilometer. Optoelectron. Instrument. Proc. 46: 198-205.

Edoardo Charbon. 2004. Will CMOS imagers ever need ultra-high speed? Proceedings. 7th International Conference on Solid-State and Integrated Circuits Technology, 2004. 3: 1975-1980.

Emil-Alexandru Brujan, Kester Nahen, Peter Schmidt *et al*. 2001. Dynamics of laser-induced cavitation bubbles near an elastic boundary. Journal of Fluid Mechanics. 433: 251-281.

Emil-Alexandru Brujan & Yoichiro Matsumoto. 2012. Collapse of micrometer-sized cavitation bubbles near a rigid boundary. Microfluid Nanofluid. 13: 957-966.

Erik T Thostenson & Tsu-Wei Chou. 2002. Aligned multi-walled carbon nanotube-reinforced composites: processing and mechanical characterization. Journal of Physics D: Applied Physics. 35: L77-L80.

Herwig Kogelnik & Tingye Li. 1966. Laser Beams and Resonators. Applied Optics. 5: 1550-1567.

Iskander Sh Akhatov, Olgert Lindau, Andrey S. Topolnikov *et al*. 2001. Collapse and rebound of a laser-induced cavitation bubble. Physics of Fluids. 13: 2805-2819.

J. E. Geusic, H. M. Marcos, & LeGrand Van Uitert. 1964. Laser oscillations in Nd-doped yttrium aluminum, yttrium gallium and gadolinium garnets. Applied Physics Letters. 4: 182-184.

Jae-hwang Lee, David Veysset, Jonathan P Singer *et al*. 2012. High strain rate deformation of layered nanocomposites. Nature Communications. 3: 1164.

Jae-Hwang Lee, Phillip E. Loya, Jun Lou *et al*. 2014. Materials science. dynamic mechanical behavior of multilayer graphene via supersonic projectile penetration. Science. 346: 1092-1096.

James C. Wyant, Chris L. Koliopoulos, Bharat Bhushan *et al*. 1984. An Optical Profilometer for Surface Characterization of Magnetic Media. A S L E Transactions. 27: 101-113.

Jessica A Zimberlin, Jennifer J McManus & Alfred J Crosby. 2010. Cavitation rheology of the vitreous: mechanical properties of biological tissue. Soft Matter. 6: 3632-3635.

Jessica A. Zimberlin, Naomi Sanabria-DeLong, Gregory N. Tew *et al*. 2007a. Cavitation rheology for soft materials. Soft Matter. 3: 763-767.

Jessica A. Zimberlin, Naomi Sanabria-DeLong, Gregory N. Tew *et al*. 2007b. Cavitation rheology for soft materials. Soft Matter. 3: 763-767.

Jinyang Liang & Lihong V. Wang. 2018. Single-shot ultrafast optical imaging. Optica, OPTICA. 5: 1113-1127.

John M. Senior & M. Yousif Jamro. 2009. Optical Fiber Communications: Principles and Practice. Pearson Education.

Jonathan B. Estrada, Carlos Barajas, David L Henann, *et al*. 2018. High strain-rate soft material characterization via inertial cavitation. Journal of the Mechanics and Physics of Solids. 112: 291-317.

M. P. Felix & A. T. Ellis. 1971. Laser-induced liquid breakdown-a step-by-step account. Applied Physics Letters. 19: 484-486.

Manfred Oehmichen, Christoph Meissner & Hans Günter König. 2000. Brain injury after gunshot wounding: morphometric analysis of cell destruction caused by temporary cavitation. Journal of Neurotrauma. 17: 155-162.

Mark Harrison. 1952. An experimental study of single bubble cavitation noise. The Journal of the Acoustical Society of America. 24: 776-782.

Massig Jurgen H., inventor; Carl Zeiss A. G., assignee. 1989. Interferometric Profilometer Sensor.

Matthew B. Panzer, Barry S. Myers, Bruce P. Capehart *et al*. 2012. Development of a finite element model for blast brain injury and the effects of CSF cavitation. Ann. Biomed. Eng. 40: 1530-1544.

Michael Plaksin, Shy Shoham & Eitan Kimmel. 2014. Intramembrane cavitation as a predictive bio-piezoelectric mechanism for ultrasonic brain stimulation. Phys. Rev. X. 4: 011004.

Monte Ross. 1968. YAG laser operation by semiconductor laser pumping. Proceedings of the IEEE. 56: 196-197.

Qiyong Chen, Arash Alizadeh, Wanting Xie *et al*. 2018. High-strain-rate material behavior and adiabatic material instability in impact of micron-scale Al-6061 particles. Journal of Thermal Spray Technology. 27: 641-653.

R. W. Klopp, R. J. Clifton & T. G. Shawki. 1985. Pressure-shear impact and the dynamic viscoplastic response of metals. Mechanics of Materials. 4: 375-385.

Richard K. Boger, Robert H. Wagoner, Frederic Barlat *et al*. 2005. Continuous, large strain, tension/compression testing of sheet material. International Journal of Plasticity. 21: 2319-2343.

Rie Tanabe, Takahiro Sugiura, Yoshiro Ito *et al*. 2015. Bubble dynamics in metal nanoparticle formation by laser ablation in liquid studied through high-speed laser stroboscopic videography. Applied Surface Science. 351: 327-331.

Robert W. Style, Callen Hyland, Rostislav Boltyanskiy *et al*. 2013. Surface tension and contact with soft elastic solids. Nature Communications. 4: 2728.

Roeland Jozef Gentil De Moor, Jan Blanken, Maarten Meire *et al*. 2009. Laser induced explosive vapor and cavitation resulting in effective irrigation of the root canal. Part 2: evaluation of the efficacy. Lasers in Surgery and Medicine. 41: 520-523.

Santanu Kundu & Alfred J. Crosby. 2009. Cavitation and fracture behavior of polyacrylamide hydrogels. Soft Matter. 5: 3963-3968.

Staffan Greek, Fredric Ericson, Stefan Johansson, *et al*. 1999. Mechanical characterization of thick polysilicon films: Young's modulus and fracture strength evaluated with microstructures. Journal of Micromechanics and Microengineering. 9: 245-251.

Sung-Yong Park, Ting-Hsiang Wu, Yue Chen *et al*. 2011. High-speed droplet generation on demand driven by pulse laser-induced cavitation. Lab Chip. 11: 1010-1012.

Tetsuya Kodama & Kazuyoshi Takayama. 1998. Dynamic behavior of bubbles during extracorporeal shock-wave lithotripsy. Ultrasound in Medicine & Biology. 24: 723-738.

U. Schnell, R. Dändliker & S. Gray. 1996. Dispersive white-light interferometry for absolute distance measurement with dielectric multilayer systems on the target. Opt. Lett. , OL. 21: 528-530.

Wanting Xie, Arash Alizadeh-Dehkharghani, Qiyong Chen *et al*. 2017. Dynamics and extreme plasticity of metallic microparticles in supersonic collisions. Scientific reports. 7: 5073-9.

World Health Organization. 2018. Global status report on road safety 2018. 2019.

Xiaodong Li, Bharat Bhushan, Kazuki Takashima *et al*. 2003. Mechanical characterization of micro/nanoscale structures for MEMS/NEMS applications using nanoindentation techniques. Ultramicroscopy. 97: 481-494.

Zhiwen Chen, Fan Yang, Hao Zheng *et al*. Dec 2018. Preparation and mechanical characterization of Ni-Fe-P coating for power electronics. : 443-446.